Atmos. Meas. Tech., 11, 291–313, 2018
https://doi.org/10.5194/amt-11-291-2018
© Author(s) 2018. This work is distributed under
the Creative Commons Attribution 4.0 License.

Atmospheric Measurement Techniques
Open Access

A machine learning calibration model using random forests to improve sensor performance for lower-cost air quality monitoring

Naomi Zimmerman[1], Albert A. Presto[1], Sriniwasa P. N. Kumar[1], Jason Gu[2], Aliaksei Hauryliuk[1], Ellis S. Robinson[1], Allen L. Robinson[1], and R. Subramanian[1]

[1]Center for Atmospheric Particle Studies, Carnegie Mellon University, Pittsburgh, PA 15213, USA
[2]Sensevere LLC, Pittsburgh, PA 15222, USA

Correspondence: R. Subramanian (subu@cmu.edu)

Received: 25 July 2017 – Discussion started: 9 August 2017
Revised: 3 November 2017 – Accepted: 20 November 2017 – Published: 15 January 2018

Abstract. Low-cost sensing strategies hold the promise of denser air quality monitoring networks, which could significantly improve our understanding of personal air pollution exposure. Additionally, low-cost air quality sensors could be deployed to areas where limited monitoring exists. However, low-cost sensors are frequently sensitive to environmental conditions and pollutant cross-sensitivities, which have historically been poorly addressed by laboratory calibrations, limiting their utility for monitoring. In this study, we investigated different calibration models for the Real-time Affordable Multi-Pollutant (RAMP) sensor package, which measures CO, NO_2, O_3, and CO_2. We explored three methods: (1) laboratory univariate linear regression, (2) empirical multiple linear regression, and (3) machine-learning-based calibration models using random forests (RF). Calibration models were developed for 16–19 RAMP monitors (varied by pollutant) using training and testing windows spanning August 2016 through February 2017 in Pittsburgh, PA, US. The random forest models matched (CO) or significantly outperformed (NO_2, CO_2, O_3) the other calibration models, and their accuracy and precision were robust over time for testing windows of up to 16 weeks. Following calibration, average mean absolute error on the testing data set from the random forest models was 38 ppb for CO (14 % relative error), 10 ppm for CO_2 (2 % relative error), 3.5 ppb for NO_2 (29 % relative error), and 3.4 ppb for O_3 (15 % relative error), and Pearson r versus the reference monitors exceeded 0.8 for most units. Model performance is explored in detail, including a quantification of model variable importance, accuracy across different concentration ranges, and performance in a range of monitoring contexts including the National Ambient Air Quality Standards (NAAQS) and the US EPA Air Sensors Guidebook recommendations of minimum data quality for personal exposure measurement. A key strength of the RF approach is that it accounts for pollutant cross-sensitivities. This highlights the importance of developing multipollutant sensor packages (as opposed to single-pollutant monitors); we determined this is especially critical for NO_2 and CO_2. The evaluation reveals that only the RF-calibrated sensors meet the US EPA Air Sensors Guidebook recommendations of minimum data quality for personal exposure measurement. We also demonstrate that the RF-model-calibrated sensors could detect differences in NO_2 concentrations between a near-road site and a suburban site less than 1.5 km away. From this study, we conclude that combining RF models with carefully controlled state-of-the-art multipollutant sensor packages as in the RAMP monitors appears to be a very promising approach to address the poor performance that has plagued low-cost air quality sensors.

1 Introduction

Historically, spatial coverage of air quality monitoring stations has been limited by the high cost of instrumentation; urban areas typically rely on a few reference-grade monitors to assess population scale exposure. However, air pollutant concentrations often exhibit significant spatial variability depending on local sources and features of the built environment (Marshall et al., 2008; Nazelle et al., 2009; Pugh et al., 2012; Tan et al., 2014), which may not be well captured by the existing monitoring networks. In the past sev-

eral years, there has been a significant increase in the development and applications of low-cost sensor-based air quality monitoring technology (Lewis and Edwards, 2016; McKercher et al., 2017; Moltchanov et al., 2015; Snyder et al., 2013). The use of low-cost air quality sensors for monitoring ambient air pollution could enable much denser air quality monitoring networks at a comparable cost to the existing regime. Increasing the spatial density of air quality monitoring would help quantify and characterize exposure gradients within urban areas and support better epidemiological models. Additionally, more highly resolved air quality information can assist regulators with future policy planning, with identification of hot spots or potential areas of concern (e.g., fracking in rural areas) where more detailed characterization is needed, and with risk mitigation for noncompliant zones. Furthermore, low-cost air quality sensors are generally characterized by their compact size and low power demand. These features enable low-cost sensors to be moved with relative ease to rural areas or developing regions where limited monitoring exists.

The two primary requirements of low-cost sensors for ambient measurement are (1) hardware that is sensitive to ambient pollutant concentrations and (2) calibration of the sensors. The latter is the focus of this study. The challenge with low-cost air quality sensor calibration is that the sensors are prone to cross-sensitivities with other ambient pollutants (Bart et al., 2014; Cross et al., 2017; Masson et al., 2015b; Mead et al., 2013). The most common example is for ozone electrochemical sensors, which also undergo redox reactions in the presence of NO_2. Additionally, NO has also been observed to interfere with NO_2, and CO sensors have exhibited some cross-sensitivity to molecular hydrogen in urban environments (Mead et al., 2013). Furthermore, low-cost sensors can be affected by meteorology (Masson et al., 2015b; Moltchanov et al., 2015; Pang et al., 2017; Williams et al., 2013). Most electrochemical sensors are configured such that the reactions are diffusion-limited, and the diffusion coefficient can be affected by temperature (Hitchman et al., 1997); Masson et al. (2015b) have shown that at relative humidity (RH) exceeding 75 % there is significant error, possibly due to condensation on potentiostat electronics. Lastly, the stability of low-cost sensors is known to degrade over time (Jiao et al., 2016; Masson et al., 2015a). For example, in electrochemical cells, the reagents are consumed over time and have a typical lifetime of 1–2 years.

Deconvolving the effects of cross-sensitivity and stability on sensor performance is complex. Linear calibration models developed in the laboratory perform poorly on ambient data (Castell et al., 2017). Attempts to build calibration models from first principles have shown some success, but the models are difficult to construct and their transferability to new environments remains unknown (Masson et al., 2015b). Accurate and precise calibration models are particularly critical to the success of dense sensor networks deployed in urban areas of developed countries where concentrations are on the low end of the spectrum of global pollutant concentrations, as poor signal-to-noise ratios and cross-sensitivities may hamper their ability to distinguish between intra-urban sites. As such, there has been increasing interest in more sophisticated algorithms (e.g., machine learning) for low-cost sensor calibration. To date, there have been published studies using high-dimensional multi-response models (Cross et al., 2017) and neural networks (Esposito et al., 2016; Spinelle et al., 2015, 2017, De Vito et al., 2008, 2009). Spinelle et al. (2015) showed that artificial neural network calibration models could meet European data quality objectives for measuring ozone (uncertainty < 18 ppb); however, meeting these objectives for NO_2 remained a challenge. In De Vito et al. (2009), the neural network calibration approach was applied to CO, NO_2, and NO_x metal oxide sensors in Italy with encouraging results; in general mean relative error was approximately 30 %. Cross et al. (2017) built high-dimensional multi-response calibration models for CO, NO, NO_2, and O_3 which had good agreement with reference monitors (slopes: 0.47–0.94; R^2: 0.39–0.88). Esposito et al. (2016) demonstrated excellent performance with dynamic neural network calibrations of NO_2 sensors (mean absolute error (MAE) < 2 ppb); however, the same performance for O_3 was not observed. Furthermore, these calibrations have only been tested on a small number of sensor packages. For example, Cross et al. (2017) tested two sensor packages, each containing one sensor per pollutant over a 4-month period, of which 35 % was used as training data. Spinelle et al. (2015) tested a cluster of sensors in a single enclosure, testing 22 individual sensors in total over a period of 5 months, of which 15 % was used as training data. Esposito et al. (2016) reported calibration performance on a single sensor package (five gas sensors per package for measuring NO, NO_2, and O_3), and the model was tested on 4 weeks of data.

In this study, we aim to improve the calibration strategies of low-cost sensors using a random-forest-based machine learning algorithm, which, to our knowledge, has not been previously applied to low-cost air quality monitor calibrations. To ensure calibration model robustness, they were developed and validated for 16–19 Real-time Affordable Multi-Pollutant (RAMP) monitors (depending on pollutant), with each monitor containing one sensor per species (CO, CO_2, NO_2, SO_2 and O_3). Furthermore, the study was conducted over a 6-month period (August 2016 to February 2017) spanning multiple seasons and a wide range of meteorological conditions. During this period, RAMP monitors were intermittently deployed for air quality monitoring campaigns, resulting in collocation periods ranging from 5.5 to 16 weeks (median: 9 weeks). The fitting of the machine learning algorithms is discussed in detail to determine ideal calibration data sets to maximize performance and minimize overtraining. The performance of the random forest (RF) models is compared to traditional laboratory univariate linear models, multiple linear regression models, and EPA performance

guidelines. The performance of a given model over time is also discussed.

2 Experimental methods

2.1 Measurement sites

Measurements were made from 3 August 2016 to 7 February 2017 on the Carnegie Mellon University campus in the Oakland neighborhood of Pittsburgh, PA, US. The outdoor ambient testing environment (40°26′31.5″ N, 79°56′33″ W) is located within a small (< 100 vehicles) limited-access, open-air parking lot near the center of campus. It consisted of a mobile laboratory equipped with reference-grade instrumentation (Sect. 2.3) and adjacent lawn space where the RAMP monitors were mounted on tripods (Sect. 2.2). The dominant local source at the site is vehicle emissions when vehicles enter and exit the parking lot during the morning and evening rush hours. There was also occasional truck traffic and restaurant emissions from nearby on-campus restaurants. The small size of the parking lot (< 100 cars) and few other local sources means that for most of the day the location is essentially an urban background site. During the measurement period, the site mean (range) ambient temperature and relative humidity were 13 °C (−15 to 34 °C) and 71 % (27 to 98 %), respectively.

The RAMP monitors have also been intermittently deployed across the Pittsburgh region as part of ongoing air quality monitoring research. To demonstrate the accuracy of the calibrated RAMP monitors, we also show data from a RAMP monitor which was first calibrated at Carnegie Mellon University and then moved to the Allegheny County Health Department (ACHD; 40°27′55.6″ N, 79°57′38.9″ W) from February to May 2017. The ACHD site has independent reference monitors for CO, NO_2, and O_3; thus comparing data from these two sites enables an independent, real-world assessment of model performance. The ACHD site is characterized by increased traffic volume, restaurant density, and industry relative to the Carnegie Mellon site.

2.2 Real-time Affordable Multi-Pollutant monitor

The study uses the RAMP monitor, which was developed in a collaboration between Carnegie Mellon University and SenSevere. The RAMP monitor uses the following commercially available electrochemical sensors from Alphasense Ltd: carbon monoxide (CO, Alphasense ID: CO-B41), nitrogen dioxide (NO_2, Alphasense ID: NO2-B43F), sulfur dioxide (SO_2, Alphasense ID: SO2-B4), and total oxidants (O_x, Alphasense ID: Ox-B431). The unit also includes a nondispersive infrared (NDIR) CO_2 sensor (SST CO2S-A) which contains built-in T (method: bandgap) and RH (method: capacitive) measurement. The experiments involved 95 individual pollutant sensors mounted in 19 unique RAMP monitors. While the collocation period spanned August 2016 to February 2017, many sensors were intermittently deployed for air quality campaigns in Pittsburgh, so the collocation period ranged from 30 days to the full study period, depending on the unit. Additionally, calibrations were not built for sensors for which reference data were below detection limits or if reference monitoring units were malfunctioning, reducing the total number of sensors in this experiment to 73, due to issues with the SO_2 and NO_2 reference monitors.

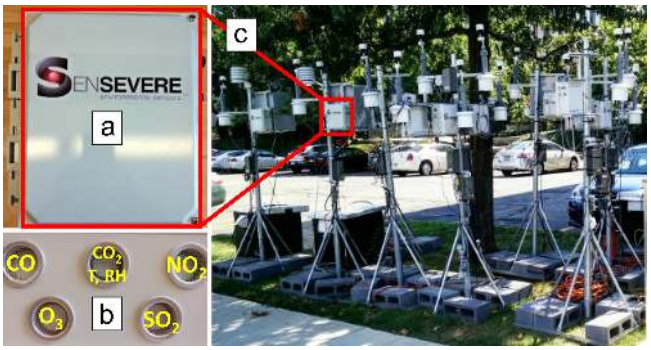

Figure 1. Photographs of the RAMP monitors and the sampling setup. **(a)** Front view of the RAMP unit in the NEMA-rated enclosure. **(b)** Bottom view of the RAMP monitors with sensor layout labeled in yellow. **(c)** Example of collocation setup using tripod mounting (not pictured: supersite containing the reference monitors, immediately beside the tripods).

The electrochemical sensor outputs were measured using electronic circuitry custom-designed by SenSevere and optimized for signal stability. The circuitry includes custom electronics to drive the device, multiple stages of filtering circuitry for specific noise signatures, and an analog-to-digital converter for measurement of the conditioned signal. The RAMP monitors are housed in a NEMA-rated weatherproof enclosure (Fig. 1a) and equipped with GSM cards to transmit data using cellular networks to an online server. The RAMP monitors also log data to a Secure Digital (SD) card as a fail-safe in case of wireless data transfer issues. The data are logged to the server at ∼ 15 s resolution and down-sampled to 15 min averages, which was deemed to be an appropriate time resolution for assessing spatial variability in air pollution exposure and to reduce the size of the data set and increase computational efficiency. Regulatory bodies typically make their data available at hourly resolution. The sensors sample passively from the bottom of the unit (Fig. 1b), with screens installed to protect the sensors. Roughly 3 weeks of measurements of gaseous species, T, and RH are possible on a single charge of a built-in 30-amp-hour nickel–metal hydride (NiMH) battery. The RAMP monitors are either mounted to a steel plate for easy pole mounting or are deployed on tripods approximately 1.5 m above the ground (Fig. 1c). In this study, all the RAMP monitors were tripod-mounted at a consistent height.

In their simplest configuration, electrochemical sensors function based on a redox reaction within an electrochemical cell in which the target analyte oxidizes the anode and the cathode is proportionally reduced (or vice versa, depending on target analyte). The subsequent movement of charge between the electrodes produces a current which is proportional to the analyte reaction rate, which can be used to determine the analyte concentration. The Alphasense electrochemical sensors utilize a more complex configuration by using four electrodes (working, reference, counter, and auxiliary) to account for zero current changes. Essentially, the auxiliary electrode, which is not exposed to the target analyte, accounts for changes in the sensor baseline signal under different meteorological conditions. Additional details on the theory of operation for electrochemical sensors can be found in Mead et al. (2013).

The RAMP monitors log two output signals from each of the Alphasense sensors: one from the auxiliary electrode and the other from the working electrode. The net sensor response is determined by subtracting the auxiliary electrode signal from that of the working electrode. In theory, for a target analyte a linear relationship should exist between the net sensor signal for that analyte and ambient analyte concentrations, and this expectation forms the basis of univariate linear regression models built from laboratory calibrations. However, as noted in the Introduction, even with an auxiliary electrode, electrochemical sensors may insufficiently account for the impacts of temperature (which affects the rate of diffusion) and relative humidity under high-humidity conditions where condensation is possible. This has motivated researchers to construct multiple linear regression (MLR) models to account for these temperature and humidity effects (Jiao et al., 2016). While these calibration models typically improve performance relative to univariate linear models (Spinelle et al., 2015, 2017), they typically do not incorporate any cross-sensitivities to other pollutants or any nonlinearities in the response. In this study, we attempt to build a calibration model for each analyte with no underlying assumptions regarding the calibration model structure and allow the models to consider directly the full suite of data being reported by the RAMP monitors using a machine learning approach.

2.3 Reference instrumentation

Reference measurements were made on ambient air continuously drawn through an inlet on the roof of the mobile laboratory located approximately 2.5 m above ground. Gaseous pollutants were drawn through approximately 4 m of 0.953 cm outer-diameter Teflon fluorinated ethylene propylene (FEP) tubing with a six-port stainless-steel manifold for flow distribution to the gas analyzers. Measurements were made using direct absorbance at 405 nm for NO_2 (2B Technologies Model 405 nm), a gas filter correlation infrared analyzer for CO (Teledyne T300U), a nondispersive infrared analyzer for CO_2 (LICOR 820), UV absorption for O_3 (Teledyne T400 Photometric Ozone Analyzer), and UV fluorescence for SO_2 (Teledyne T100A UV Fluorescence SO_2 Analyzer). The time resolution for all reference measurements was 1 s.

The reference gas analyzers were checked and calibrated weekly using calibration gas mixtures, except for O_3, which is calibrated biannually at a nearby regulatory monitoring site. The CO and NO_2 analyzers experience modest baseline drift between weekly calibrations, on the order of approximately 40 ppb for CO and 2 ppb for NO_2. Hence, baseline pollutant concentrations were normalized to a nearby regulatory monitoring site (Allegheny County Health Department, Air Quality Division, Pittsburgh, PA, US). The baseline correction was done using a linear regression between the beginning and end of the week on the baseline signals (local source spikes removed). The regression was based on daytime differences, as nighttime inversions may cause real differences in the baseline signals between the two sites. The gas analyzers at the regulatory monitoring site are checked daily, and thus this normalization helped correct for any baseline drift during the days between calibration. No significant drift was observed for CO_2 or O_3.

3 Calibration methods

Three calibration methods were evaluated: (1) a laboratory-based univariate linear regression based on net sensor response when exposed to calibration gases; (2) an empirical multiple linear regression of net sensor response, T, and RH regressed against reference monitor concentrations; and (3) a random forest machine learning model using net responses from all sensors, T, and RH to predict reference monitor concentrations. Calibration models were constructed for the CO, NO_2, CO_2, and O_3 sensors in each RAMP monitor. In this study, no calibration models were built for SO_2 due to a combination of reference instrument malfunction and SO_2 concentrations measured with the reference instrumentation being below the instrument detection limit (< 0.4 ppbv) for most of the campaign (no nearby sources of SO_2). While lab calibrations were conducted for the SO_2 sensors, these data will be the subject of a future publication on air quality in industrial areas where SO_2 is more commonly detected.

3.1 Laboratory-based univariate linear regression (LAB)

Prior to outdoor collocation, the sensors inside the RAMP monitors were calibrated in a laboratory environment using a custom-manufactured sensor bed and calibration gas mixtures. The sensors were exposed to each step in the calibration window (Table 1) for 20 min, and a face velocity of $1.2\,\mathrm{m\,s^{-1}}$ flowed perpendicular to the sensor surface. This face velocity is at the lower end of the wind speed

Table 1. Calibration ranges for laboratory-based calibration (LAB).

Pollutant	Calibration range	Points per calibration
CO	0–1600 ppb	3–4
NO_2	0–50 ppb	3–4
CO_2	0–500 ppm	3–4

range in Pittsburgh, PA (e.g., average monthly windspeed over January–May 2017 at 2 m height is estimated at 2.4–3.4 $m\,s^{-1}$). The sensor response at each calibration step was averaged once the signal had stabilized (steady sensor output voltage). Temperature and relative humidity were not controlled during the calibration due to a lack of available infrastructure at the time of the study. The temperature was at levels typical of indoor laboratory environments (approximately 20 °C), and the dry calibration gas provided very little humidity (RH < 5 %). Calibrations were built for CO, NO_2 and CO_2. Laboratory calibrations for O_3 were not performed due to a lack of suitable O_3 calibration gas.

The laboratory calibration follows a standard univariate linear regression model of regression net (CO, NO_2) or raw (CO_2) signal against the reference gas concentration (Eq. 1):

$$y_{\text{reference}}(t) = \beta_0 + \beta_1 \times \big[\text{net sensor resp. (CO, NO}_2\text{)} \text{ or raw sensor resp. (CO}_2\text{)}\big]. \quad (1)$$

Model performance was evaluated by comparing the calibrated response to reference measurements. We refer to the laboratory univariate linear regression calibration as LAB. Separate LAB calibrations were developed for each sensor (37 individual calibrations, 9–14 per pollutant). Due to difficulty controlling temperature and RH over a wide range of known ambient conditions, we focused on the relationship between analyte response and the calibration gas concentration, which any user with access to basic lab infrastructure can do. While beyond the scope of this study, an improved LAB calibration would involve a chamber with variable T and RH to better match ambient conditions.

3.2 Empirical multiple linear regression

Following laboratory calibration, the individual sensors were mounted in the RAMP monitors and deployed outdoors adjacent to the Carnegie Mellon University supersite. The collocation period varied by RAMP monitors, with a minimum collocation period of 6 weeks and a maximum collocation period of the entire 6-month study period. The collocation window varied due to intermittent deployment of some RAMP monitors for ongoing air quality monitoring campaigns in the Pittsburgh area. To build calibration models, the collocation period was separated into a training and testing period identical to that used for the random forest calibration (see Sect. 3.3). Due to the previously established influence of T and RH on sensor response (Jiao et al., 2016; Masson et al., 2015b; Spinelle et al., 2015, 2017), a MLR model was used to calibrate the output from each sensor using net sensor response to the target analyte (e.g., CO for the CO sensor), T, and RH as explanatory variables (Eq. 2), similar to the approach described in a recent a European Union report on protocols for evaluating and calibrating low-cost sensors (Spinelle et al., 2013).

$$\begin{aligned} y_{\text{reference}}(t) = {} & \beta_0 \\ & + \beta_1 \times \big[\text{net sensor resp. (CO, NO}_2\text{, O}_3\text{)} \\ & \quad \text{or raw sensor resp. (CO}_2\text{)}\big] \\ & + \beta_2 \times T + \beta_3 \times \text{RH} \end{aligned} \quad (2)$$

The training data were used to calculate the model coefficients (β_0 through β_3), and the model performance was evaluated on withheld testing data. Separate MLR models were developed for each sensor (73 individual models). We refer to these models as MLR.

3.3 Random forest model

An RF model is a machine learning algorithm for solving regression or classification problems (Breiman, 2001). It works by constructing an ensemble of decision trees using a training data set; the mean value from that ensemble of decision trees is then used to predict the value for new input data. Briefly, to develop a random forest model, the user specifies the maximum number of trees that make up the forest, and each tree is constructed using a bootstrapped random sample from the training data set. The origin node of the decision tree is split into sub-nodes by considering a random subset of the possible explanatory variables (m_{try}). The training algorithm splits the tree based on which of the explanatory variables in each random subset is the strongest predictor of the response. The number of random explanatory variables considered at each node (denoted m_{try}) is tuned by the user. This process of node splitting is repeated until a terminal node is reached; the user can specify the maximum number of sub-nodes or the minimum number of data points in the node as the indication to terminate the tree. For our random forest models, the terminal node was specified using a minimum node size of five data points per node.

To illustrate the method, consider building a random forest model for one RAMP monitor using a single decision tree and a subset of 100 training data points to build a CO calibration model (Fig. 2). In this highly simplified example, at the first node, the net CO sensor signal is the strongest predictor of the CO reference monitor concentration, with a natural split in the data at a net CO sensor voltage of 255.9 a.u. (arbitrary units) If sensor voltage exceeds 255.9 a.u., a cluster of seven data points from the training data predicts an average CO concentration of 357 ppb; if CO net sensor voltage is $\leq$ 255.9 a.u., then the data go to the next decision node, in which net CO sensor signal is again the strongest predictor of the CO reference monitor concentration, with a natural

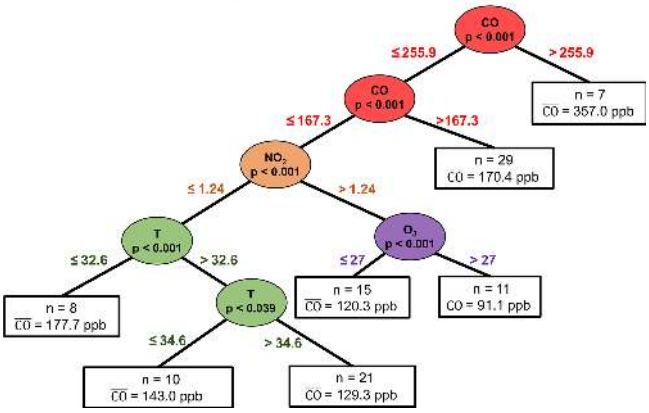

Figure 2. Simplified illustration of one potential CO random forest tree for one RAMP monitor using 100 data points (the trees within the actual models are significantly more complex, and 500 such trees are included in the final models). Tree nodes are colored by splitting variable, and split point is overlaid on the branch (e.g., at first split, points with CO sensor signal > 255.9 a.u. are sent to a terminal node; the remaining points go to the next splitting node). $\overline{\mathrm{CO}}$ is the average CO reference monitor concentration (ppb) in each terminal node; n is the number of data points in each terminal node.

break in the data at a net CO sensor voltage of 167.3 a.u. The splitting proceeds until all the training data are assigned to a terminal node. The prediction value for each terminal node is the average reference monitor concentration of training points assigned to that node. To apply the algorithm (i.e., predict the CO concentration from a set of measured inputs), the user takes the measured T and the net CO, NO_2, and O_3 signals and follows the path through the tree to the appropriate terminal node. The predicted CO concentration for that tree is then the average training value associated with that terminal node. This process is then repeated through multiple trees (Fig. 2 shows only one simple tree), and the predictions from each tree are averaged to determine the final output from the entire random forest model. In this simple example, there are only six possible CO concentrations the random forest model will output. In practice, each tree has hundreds of terminal nodes and the forest typically comprises hundreds of trees, which means that there are thousands of possible answers. The model prediction for a given set of inputs is the average prediction across all the hundreds of trees that comprise the forest.

The random forest model's critical limitation is that its ability to predict new outcomes is limited to the range of the training data set; in other words, it will not predict data with variable parameters outside the training range (no extrapolation). Therefore, a larger and more variable training data set should create a better final model. In this study, our collocation window covered a broad range of concentrations and meteorological conditions; however, in situations where shorter collocation windows with less diverse training ranges are desired, the RF model may not be suitable as a standalone model. This is discussed further in Sect. 4.3.2. To maximize utilization of the training data set to avoid missing any spikes during the training window, a k-fold cross-validation approach was used. A k-fold cross-validation divides the data into k equal-sized groups (where k is specified by the user), and k repeats are used to tune the model. Consider an example where k is equal to 5 (a fivefold cross-validated random forest model). With a fivefold validation, five unique random forest models are constructed, one for each fold. In building the first random forest, the first 20 % $(1/k)$ of the data will be the testing data, and the remaining 80 % $[(1-k)/k]$ of the data will be used as training. In building the second random forest, the next 20 % of the data will be used as test data, and the first 20 % and remaining 60 % will be used to train. This is repeated until the data are fully covered, at which point the random forest model is created by combining the five (k) individual models into one large random forest model. This helps to minimize bias in training data selection when predicting new data and ensures that every point in the training window is used to build the model.

In this study, reference gas data; RAMP net sensor data for CO, NO_2, SO_2, and O_3; and RAMP raw sensor data for CO_2, T, and RH were collected at 15 s resolution, time-matched, and down-averaged to 15 min intervals (IGOR Pro v6.34), which is a higher temporal resolution than the 1 h intervals at which typical regulatory monitoring information is reported and minimized computational cost. The down-sampled data were then imported into R (ver. 3.3.3, "Another Canoe") for random forest model building. R is an open-source package for tuning and cross-validating many classes of statistical models, including random forest models. The cross-validated random forest models were compiled using the open-source "caret" package (Kuhn et al., 2017). The model considered all RAMP data (net voltage outputs from the five gas sensors plus T and RH: seven possible variables total) as potential explanatory variables to predict the reference monitor gas concentration. The number of trees was capped at 100 per fold, and a fivefold cross-validation was used for a total of 500 trees. Therefore, the predicted value for a given set of measured inputs is the average value from this set of 500 trees (each tree provides one prediction). The k value was chosen by identifying the minimum number of folds for which an increase in the fold size increased model performance less than 5 % on the held-out data. The number of trees was chosen based on the work of Oshiro et al. (2012), who suggested that the number of trees range from 64 to 128. The computation time to train a complete RAMP monitor with five sensors was approximately 45 min. This was another motivating factor for 15 min resolution data, as building models at higher time resolutions would have significantly increased computational demand.

When fitting the random forest models with the training data, the main tuning parameter is the number of explanatory variables to consider at each decision node (m_{try}). To deter-

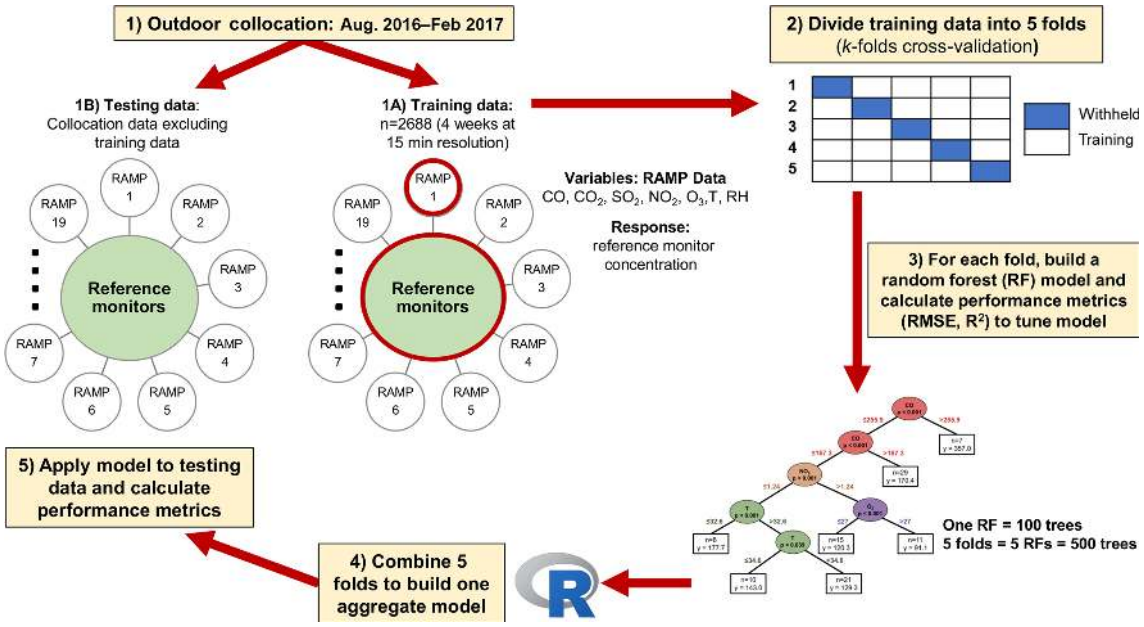

Figure 3. Flow path for data collection and RF model fitting and testing. From collocation period, 2688 points were sub-selected as training (1A) data, while the remaining data were used for model testing (1B). The training data were further divided into five cross-validation folds, and each fold was used to tune and build an RF model. All five models were then combined in R to build one cumulative model, and the predictive power of the model was assessed for the withheld testing data.

mine the optimal m_{try}, the root mean square error (RMSE, equation in the Supplement) and the coefficient of determination (R^2) were calculated on the withheld folds of the training data (Fig. 3, step 2) for m_{try} equal to 2, 4, or 7 to span the complete variable range. The random subset of explanatory variables considered at each node was chosen based on which value of m_{try} minimized RMSE. The cross-validation and the subset of explanatory variables randomly considered at each node (m_{try}) was tuned using the caret package in R (Kuhn et al., 2017). Following random forest model generation and tuning, the five 100-tree models were combined to create a final model with 500 trees. This process was repeated for each sensor to create 73 separate random forest models. The final models convert the RAMP output signals into calibrated concentrations. The model conversion was done within R, where it exists as a standalone object compatible with the standard R configuration.

Data from three RAMP monitors (15 individual gas sensors) were used to investigate the optimal training period, which was determined by comparing the training data size to MAE (the average of the absolute value of the residuals). The optimal training period was the period beyond which increases in the length of the training window (and therefore size of the training dateset) no longer resulted in significant reductions in the MAE. The initial training window evaluated was 1 week, and 1-week increments in training period duration were considered until MAE was minimized. The optimal collocation window was determined to be 4 weeks (or 2688 data points at 15 min resolution). This was evaluated for a consecutive collocation window and for eight non-consecutive collocation windows equally distributed throughout the whole collocation period (August 2016 to February 2017) in half-week increments. Details of this evaluation are provided in the Supplement, but the non-consecutive collocations generally performed slightly better, with reductions in MAE of 12 ppb (4 % relative error) for CO, 2 ppm for CO_2 (0.4 % relative error), 0.4 ppb for NO_2 (4 % relative error), and 1.6 ppb for O_3 (7 % relative error) compared to the consecutive 4-week collocation. The motivation for exploring non-consecutive collocation windows dispersed throughout the study period was to ensure that the training period covered a complete range of gas species concentrations, temperatures, and relative humidity. In practice, the training data utilized in this study are equivalent to collocating the RAMP monitors with reference monitors for 3–4 days every 1–2 months. If non-consecutive collocation is inconvenient or not possible, consecutive collocation may be satisfactory as determined by MAE and other accuracy parameters needed for the application at hand.

3.4 Metrics for performance evaluation

The evaluation of the different models was conducted on 15 min averaged testing data (i.e., data withheld entirely from model building). Metrics to quantitatively compare the LAB, MLR, and RF model output to the reference monitor concentrations included Pearson r, which is a measure of the strength and direction of a linear relationship, and the co-

efficient of variation of the mean absolute error (CvMAE, Eq. 3). For comparing the RF model performance to other published studies, we also evaluated mean bias error, mean absolute error, slope of the linear regression of RF-model-calibrated RAMP data and reference data, and coefficient of determination (R^2).

$$\mathrm{CvMAE} = \frac{\mathrm{MAE}}{\text{avg. reference conc.}} = \frac{1}{\text{avg. reference conc.}} \times \left[\frac{1}{n} \sum_{i=1}^{n} |\mathrm{model}_i - \mathrm{reference}_i| \right] \quad (3)$$

Another useful tool for visually comparing competing models is a target diagram (Jolliff et al., 2009). A target diagram illustrates the contributions of the centered root mean square error (CRMSE, which is RMSE corrected for bias) and the mean bias error (MBE) towards total RMSE. In a target diagram, the x axis is the CRMSE, the y axis is the MBE, and the vector distance to the origin is the RMSE. Since CRMSE is always positive, a further dimension is added: if the standard deviation of the model predictions (calibrated sensor data) exceeds the standard deviation of the reference measurements, the CRMSE is plotted in the right quadrants and vice versa. To match previously constructed target diagrams (Borrego et al., 2016; Spinelle et al., 2015, 2017), the CRMSE and MBE were normalized by the standard deviation of the reference measurements, and thus the vector distance in our diagrams is $\mathrm{RMSE}/\sigma_{\mathrm{reference}}$(nRMSE). The resulting diagram enables visualization of four diagnostic measures: (1) whether the model tends to overestimate (MBE > 0) or underestimate (MBE < 0); (2) whether the standard deviation of the model predictions (calibrated sensor data) is larger (right plane) or smaller (left plane) than the standard deviation of the reference measurements; (3) whether the variance of the residuals is smaller than the variance of the reference measurements (inside circle of radius 1) or larger than the variance of the reference measurements (outside circle); and (4) the error (nRMSE), i.e., the vector distance between the coordinate and the origin. Details of equations required to build a target diagram are provided in the Supplement. Model performance metrics were calculated in R (ver. 3.3.3, Another Canoe) using the "tdr" package (Perpinan Lamigueiro, 2015).

4 Results and discussion

4.1 Calibration model goodness of fit: comparing model predictions to training data

Following model building, the goodness of fit between the model output concentrations and the reference monitor concentrations during the training window (i.e., the data used to build the model) were evaluated for all three calibration model approaches (laboratory univariate linear regression, or "LAB"; field-based multiple linear regression, or "MLR"; and field-based random forest, or "RF"). For the training period, the calibrated CO and O_3 concentrations were all highly correlated (Pearson $r > 0.8$) with the reference monitor concentrations for all the calibration model approaches (Table 2). However, only the RF model achieved strong correlations between the reference monitor and the RAMP monitors for NO_2 and CO_2 (Pearson r: 0.99). Furthermore, CvMAE for each species was $\leq 5\,\%$ during the training window for the RF models, substantially outperforming the other models.

Regression plots for 19 RAMP monitors and for CO, CO_2, and O_3 and 16 RAMP monitors for NO_2 illustrating the goodness of fit of the RF model are provided in the Supplement (Figs. S3–S6). Only 16 of the 19 RAMP monitors had an NO_2 calibration, since the NO_2 monitor malfunctioned during the period when three RAMP monitors were collocated, and so a calibration model could not be built for NO_2 for these three RAMP monitors. For the RF models, Table 2 also provides the random subset of explanatory variables sampled for splitting at each decision node (m_{try}) to achieve the lowest model RMSE. In general, the larger the m_{try}, the simpler the underlying structure of the model. For example, if there is one dominant variable but the model is permitted to consider all seven explanatory variables at each decision node (i.e., $m_{\mathrm{try}} = 7$), then the model will most frequently split the data based on the dominant variable. By contrast, the advantage of a lower m_{try} is that subtle relationships between explanatory variables and the response can be probed. When randomly selecting fewer explanatory variables ($m_{\mathrm{try}} = 2$ or 4) at each decision node, the probability of selecting a dominant variable decreases and the model is forced to split the data into sub-nodes based on variables which may have a smaller (but real) effect on the response. If the goodness of fit of the calibration model is improved by decreasing m_{try}, this suggests more complex variable interactions with the response (Strobl et al., 2008).

Using the m_{try} metric, we observed that the underlying RF model structure is the simplest for CO, that some model explanatory variable complexities exist for the O_3 and NO_2 models, and that the CO_2 model is the most complex and relies on subtle relationships between the explanatory variables to best fit the data (lowest m_{try} had the best results). This finding matches our expectations based on the LAB and MLR models; these simpler models performed best for CO and worst for CO_2. The trends in the m_{try} metric highlights the value of the RF model approach which directly accounts for multiple pollutants. This appears to be critical for O_3, NO_2 and CO_2 sensors because they are cross-sensitive to other pollutants. Cross-sensitivities have been shown to have a minimal impact on CO sensors, with the only notable cross-sensitivity being to molecular hydrogen (Mead et al., 2013). The poor performance of linear models at predicting CO_2 concentration is not surprising, as the sensor was observed to measure high concentrations under periods of high relative humidity (e.g., during rain) and in some cases during heavy rain will be saturated at 2000 ppm, the upper limit of the sen-

Table 2. Performance metrics for fits to training data (i.e., goodness of fit) discussed in Sect. 4.1.

Type	Species	No. of RAMP monitors	Avg. Pearson r (± SD)	Avg. MAE (± SD)	Avg. CvMAE (± SD)	β_0 (± SD)	β_1 (± SD)	β_2 (± SD)	β_3 (± SD)
LAB	CO	9	0.99 (± 0.01)	132 (± 32 ppb)	38 % (± 17 %)	−119 (± 53)	0.82 (± 0.69)	–	–
	CO_2	14	0.99 (± 0.01)	28 (± 24 ppm)	24 % (± 12 %)	20 (± 36)	0.98 (± 0.13)	–	–
	NO_2	14	0.99 (± 0.01)	35 (± 8 ppb)	188 % (± 48 %)	−14 (± 4.9)	0.62 (± 0.15)	–	–
MLR	CO	19	0.94 (± 0.06)	39 (± 13 ppb)	15 % (± 5 %)	32 (± 50)	1.3 (± 0.2)	−1.1 (± 2.8)	−0.1 (± 0.6)
	NO_2	16	0.59 (± 0.17)	4.6 (± 0.7 ppb)	42 % (± 5 %)	3.9 (± 16)	1.2 (± 0.5)	0.1 (± 0.3)	−0.1 (± 0.2)
	O_3	19	0.81 (± 0.06)	5.1 (± 0.6 ppb)	24 % (± 2 %)	9.4 (± 14)	0.92 (± 0.2)	0.1 (± 0.2)	−0.2 (± 0.2)
	CO_2	19	0.49 (± 0.13)	19 (± 3 ppm)	4 % (± 1 %)	390 (± 72)	0.1 (± 0.1)	−0.8 (± 0.7)	0.1 (± 1.0)
						Median m_{try}	$m_{try} = 2$	$m_{try} = 4$	$m_{try} = 7$
RF	CO	19	0.99 (± 0.00)	7.9 (± 1.5 ppb)	3 % (± 0.5 %)	7	11 %	21 %	68 %
	NO_2	16	0.99 (± 0.01)	0.5 (± 0.1 ppb)	5 % (± 1 %)	4	21 %	74 %	5 %
	O_3	19	0.99 (± 0.00)	0.7 (± 0.1 ppb)	3 % (± 0.4 %)	4	0 %	84 %	16 %
	CO_2	19	0.99 (± 0.00)	1.7 (± 0.3 ppm)	0.4 % (± 0.1 %)	2	74 %	21 %	5 %

LAB: laboratory calibration (Eq. 1); MLR: multiple linear regression (Eq. 2); RF: random forest model. For the LAB and MLR models, the fit coefficients are provided. For the RF models, the median m_{try} value across the 16–19 RAMP monitors and the breakdown of the m_{try} tuning results (m_{try} which minimized RMSE) across the 16–19 RAMP results are provided.

sor, and then is reset to 400 ppm daily, as per manufacturer recommendations. The increase in CO_2 under high-humidity conditions is likely due to the interference of water with CO_2 in the NDIR signal. Linear models are poorly suited to describe this behavior.

4.2 Evaluation of models using testing data

To test the performance of the three different calibration models, the models were applied to the testing data that were not used for model fitting. The RAMP monitor concentrations after correction using the calibration models were compared to the actual measured reference concentrations (Fig. 3, step 5). To illustrate the approach, in Fig. 4 we show a very short time series of the testing data (∼ 48 h window) for RAMP #1. This RAMP monitor's performance is representative of the average model performance across the RAMP monitors and therefore illustrates the quality of an average model. Figure 4 also shows the calibrated RAMP #1 output regressed against the reference monitor concentration for the entire testing period for all three calibration models (LAB, MLR, and RF). For this period, the RF model outperformed the LAB and MLR models for all pollutants except for CO. Differences between the different models were smallest for CO and O_3 and largest for CO_2 and NO_2; the LAB models essentially did not reproduce the reference concentrations for CO_2 and NO_2. To illustrate the consistency of the RF-model-calibrated RAMP monitors across the entire suite of monitors, regressions for all the RAMP monitors for O_3 are shown in Fig. 5. Regression plots for all RAMP monitors across the other gases are provided in the Supplement (Figs. S7–S10).

In this study, any data remaining after training were used to test model performance, provided there was at least 48 h of testing data (192 data points, each point a 15 min average). The RAMP sensors that met this threshold and are used to test the model – 16 for CO and O_3, 15 for CO_2, and 10 for NO_2 – had at least 1.4 weeks and a maximum of 15 weeks of testing data, with a median testing data set of 5 weeks. The amount of data used to test model performance varied by RAMP monitor and by pollutant because reference monitors were occasionally offline for maintenance and calibration, and some RAMP monitors were intermittently deployed for concurrent air quality monitoring campaigns in Pittsburgh. Figure S11 shows examples of testing periods for two RAMP monitors, one at the low end (#19 with ∼ 2300 testing data points) and one at the high end (#4 with ∼ 10 000 data points), interspersed with training periods (2688 data points for each sensor.)

To assess the overall model performance, two performance metrics (Pearson r and CvMAE) were calculated for each RAMP monitor using the entire testing data set (Fig. 6). The aggregate assessment shows that the MLR and RF models are interchangeable for CO, as both models achieved Pearson $r > 0.9$ and CvMAE < 15 %. The LAB model achieved a similar Pearson r, but CvMAE doubled to ∼ 30 %. For CO_2, NO_2, and O_3, the RF model substantially outperforms the LAB and MLR calibration models on the testing data. On average, Pearson r exceeded 0.8 for the RF model for CO_2 and NO_2 versus < 0.6 for the LAB and MLR calibration models. Furthermore, the RF model performance was more consistent across the RAMP monitors than the MLR and LAB models. For example, the Pearson r for O_3 ranged from 0.92 to 0.95 for the RF models versus 0.74 to 0.89 for the MLR models. This means that essentially all the RF models for O_3 performed well versus only a subset of the MLR models. The consistency of the different models is indicated by the smaller range in the box plots of Fig. 6.

To compare the LAB, MLR, and RF models, target diagrams were constructed for the four gases using all three calibration models for each RAMP monitor (Fig. 7). The target diagrams show that, on average, across the RAMP moni-

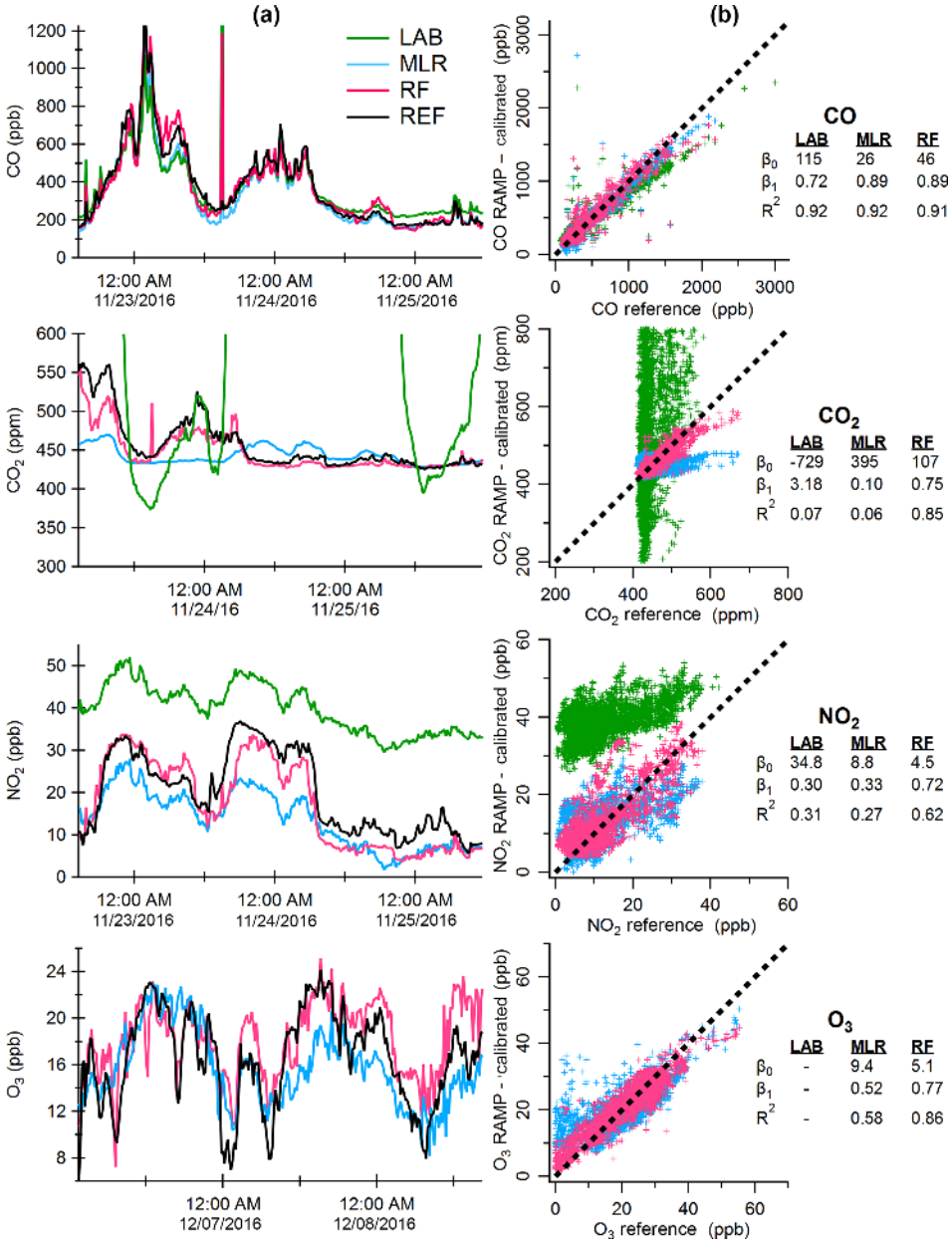

Figure 4. Example time series and regressions comparing the reference monitor data (black) to statistically average RAMP (RAMP #1) using LAB model (green), multiple linear regression (MLR) model (blue), and random forest (RF) model (pink). The left panel **(a)** shows only 48 h of time series data to illustrate the approach; the full evaluations (Table 3) were performed with much larger testing data sets; example regressions from the full data set for RAMP #1 are shown in the right panel **(b)**.

tors the random sensor error (distance to origin) was smaller for RF models, and the RF models showed the least RAMP-to-RAMP variability (less disperse). This contrasts with the MLR models, whose bias and extent of model standard deviation varied much more widely between RAMP monitors, especially for CO_2. For the LAB models, the error for CO_2 and NO_2 was approximately an order of magnitude larger than for the RF and MLR models and had to be plotted on a separate inset due to their poor performance. Across all gases, the RF models on average were biased towards predicting concentrations slightly lower than the reference (i.e., slight tendency to underpredict, $\mathrm{MBE}/\sigma_{\mathrm{reference}} < 0$). Thus, we conclude that the low CvMAE, high Pearson r correlations, lowest bias, and lowest absolute error characteristics of the RF models for all four gases are significant improvements compared to conventional calibration approaches (LAB and MLR).

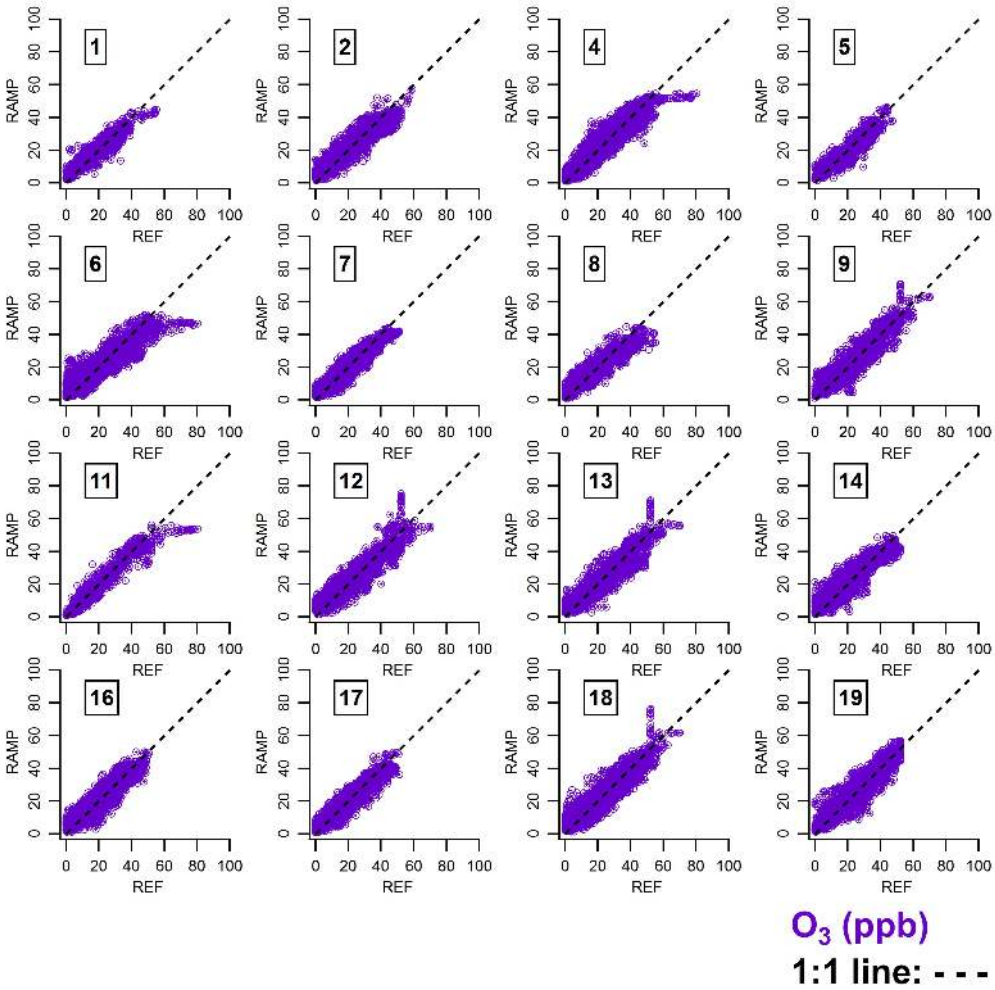

Figure 5. RF model performance for ozone evaluated using the testing data (data withheld from building model). Correlation plots show predicted ozone concentration ("RAMP") versus the reference monitor concentration ("REF") for 16 RAMP units. All values are in ppb, and the 1 : 1 line is drawn as a black dashed line.

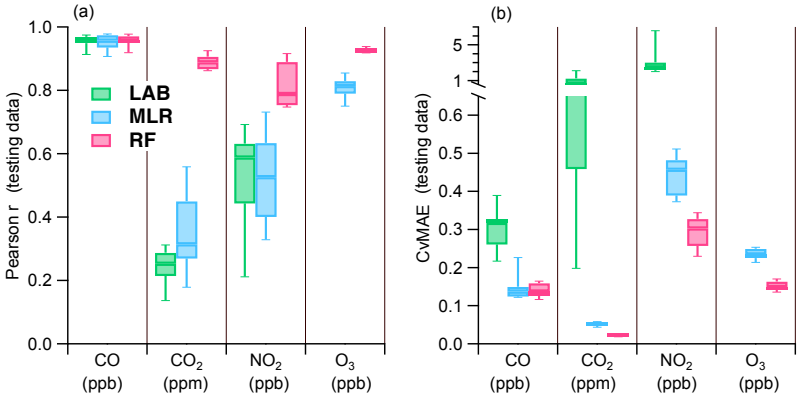

Figure 6. Performance of different calibration models against reference monitor testing data (data not included in model fitting). **(a)** Pearson *r* correlation coefficient (higher is better, maximum of 1) of different calibration models ("LAB", green; "MLR", blue; "RF", pink) versus reference monitor. **(b)** The CvMAE (coefficient of variation of the MAE; MAE normalized by average reference concentration; lower is better) for the three calibration methods. The box plots show the range across the 10–16 RAMP monitors (whiskers: 10th and 90th percentile; box edges: 25th and 75th percentile).

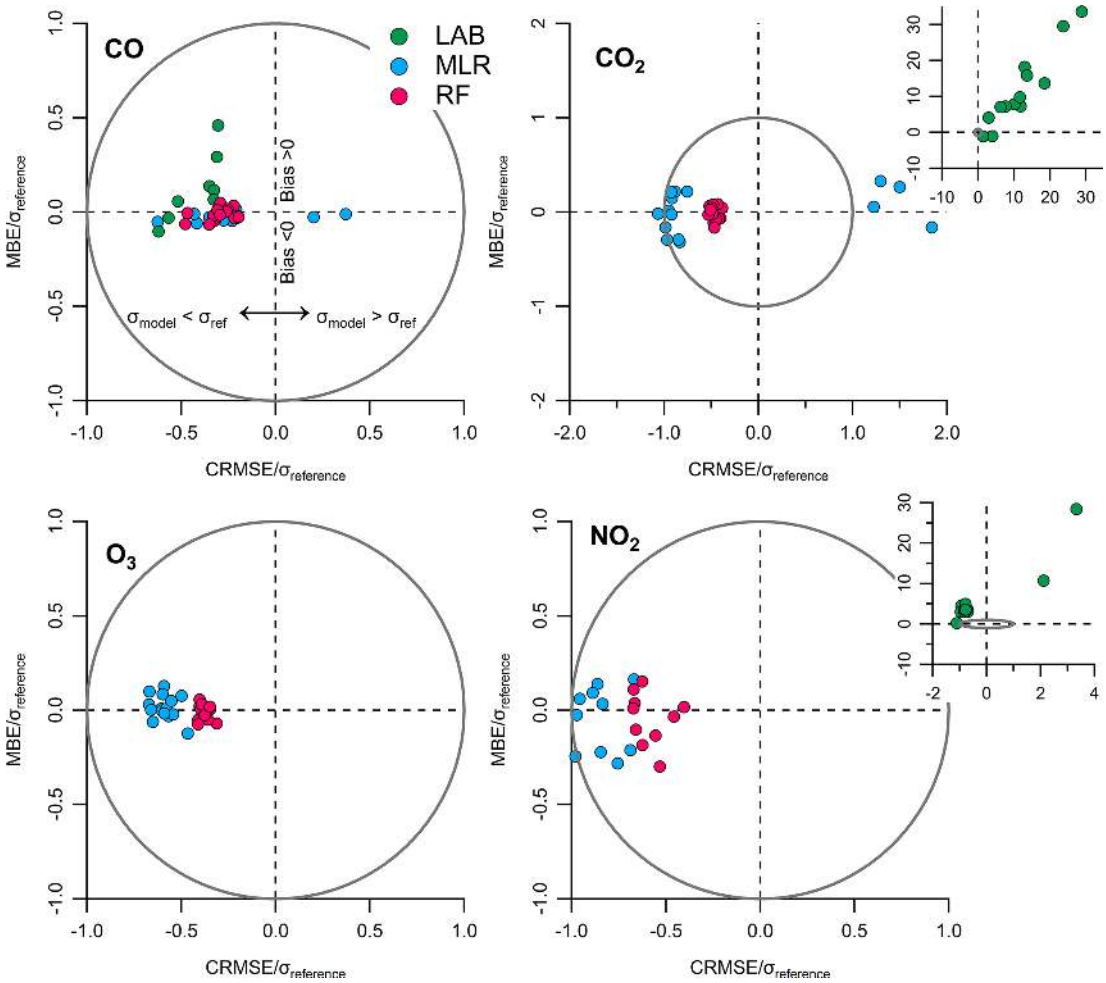

Figure 7. Target diagrams for CO, CO_2, NO_2, and O_3 to compare the LAB, MLR, and RF model performance. The *y* axis is the bias relative to the reference, and the *x* axis is the bias-adjusted RMSE (CRMSE) normalized by reference monitor standard deviation; the vector distance between any given point and the origin is the RMSE normalized by the standard deviation of the reference measurements. The CRMSE is in the left plane if model standard deviation is smaller than the standard deviation of the reference observations, and vice versa. If data fall within the circle, then the variance of the residuals is smaller than the variance of the reference measurements. The target diagram for the LAB model for CO_2 and NO_2 is shown in the inset figure because of the order-of-magnitude difference in MBE and CRMSE compared to the MLR and RF models.

4.3 Detailed assessment of RF model performance

To investigate the performance of the RF models in greater detail, we assessed the effect of the amount of testing data on model performance, the relative importance of the seven explanatory variables, the performance of the models across the different concentration ranges, and the number of data points needed in each concentration range to optimize the fit.

4.3.1 Drift over amount of testing data

To assess the effect of testing window size on conclusions regarding RF model performance, we compare the MAE to the number of weeks in the testing window (Fig. 8). For all the gas species, the MAE was essentially flat across the RAMP monitors, and the 95 % confidence interval on the slope included 0; RAMP monitors with more testing data did not have substantially higher (worse) MAE, suggesting the RF models are robust over the study period. For NO_2, the most data available for testing amounted to approximately 8 weeks due to instrument maintenance and repair taking the NO_2 reference monitor offline for 6 weeks of the study. Figure 8 also shows MAE over time from one RAMP monitor, RAMP #4, which remained at the Carnegie Mellon supersite for the entirety of the 6-month study. For RAMP #4, MAE was calculated for an increasing cumulative number of weeks forward in time; again, MAE was consistent (and in some weeks improved) over time.

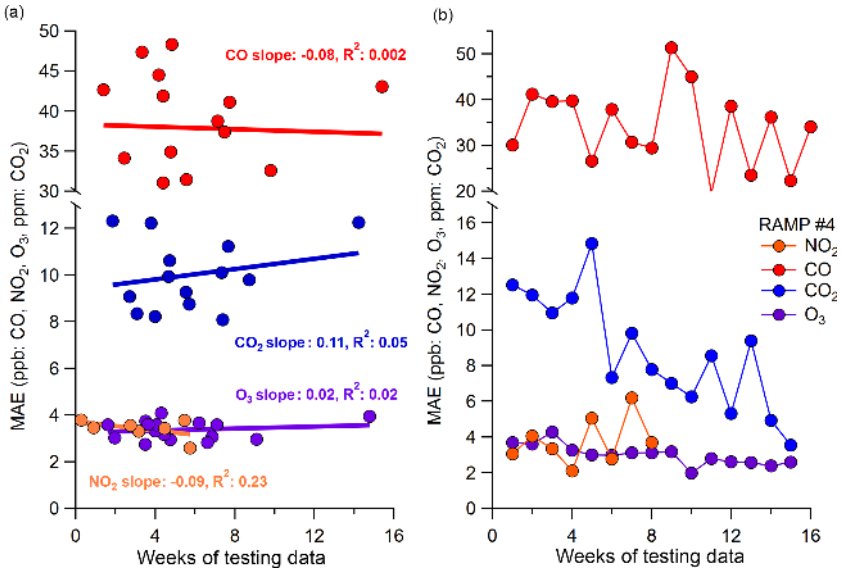

Figure 8. (a) Mean absolute error (MAE) versus the length of the testing period for CO (red), CO_2 (blue), NO_2 (orange), and O_3 (purple) for all the RAMP monitors. **(b)** Changes in MAE over time for the RAMP monitor with the longest testing window (RAMP #4). The figure shows that the MAE is generally unchanged (or in some cases improves) as the amount of testing data increases, suggesting the RF models are stable over the study period.

4.3.2 RF model explanatory variable importance

While RF models are non-parametric, some sense of the model structure can be gained by examining the relative importance of the explanatory variables. The importance of each variable was quantified by comparing the percent increase in mean square error (MSE) when an explanatory variable signal is permuted – i.e., the values of the selected variable are randomly shuffled, effectively eliminating this variable from the model (Pearson, 2017). If an explanatory variable strongly affects the model performance, permuting that variable results in a large increase in MSE. Conversely, if a variable is not a strong predictor of the response, then permuting the variable does not significantly increase the MSE. Figure 9 shows for each of the gases (CO, CO_2, NO_2, and O_3) the increase in MSE when the explanatory variables were permuted. For both CO and O_3, the signal from the sensor measuring the target analyte (CO or O_3) is the most important explanatory variable, as expected. For the O_3, the second-most-important variable was the NO_2 signal, an expected cross-sensitivity, as the ozone sensor measures total oxidants ($O_3 + NO_2$) (Spinelle et al., 2015).

The explanatory variable importance is more complex for CO_2 and NO_2. For CO_2, all variables are roughly equally important, with CO being the most important. This is likely due to the strong meteorological effect of humidity on the measured CO_2 concentration; the model must rely on other primary pollutants to predict the CO_2 signal when the measured CO_2 has reached full scale (i.e., becomes saturated in periods of high humidity), and short-term fluctuations of CO_2 are likely from combustion sources (e.g., vehicular traffic in urban areas) which also emit CO. This highlights the value of having sensors for multiple pollutants in the same monitor. Including measurements of additional pollutants helps the RF model correct for cross-sensitivities. However, the drawback of this cross-sensitivity in the model is that the RF model may not perform well in areas where the characteristic source ratios of CO and CO_2 have changed. For example, this model was calibrated in an urban environment with many traffic and combustion-related sources nearby. Such a model would be expected to perform poorly for CO_2 in a heavily vegetated rural environment where CO and CO_2 are not strongly linked. For the NO_2 model, RH was the most important explanatory variable followed by the NO_2 sensor signal, highlighting again the importance of including meteorological data within sensor packages. The NO_2 model was also more strongly affected by temperature than the other pollutants. We hypothesize that the sensitivity of the NO_2 sensor to ambient NO_2 is suppressed in Pittsburgh, which has low ambient NO_2 concentrations compared to other cities where these sensors have been evaluated (see Table 3). NO_2 is lowest when O_3 is highest in the summer, and thus the NO_2 RF model effectively uses T and RH as indicators for seasonality when NO_2 is low and the sensor response is supressed. Furthermore, the relatively equal variable importance of several of the explanatory variables within a model suggests that a cluster of sensors measuring many different species is critically important to build robust calibration models. Interestingly, despite low SO_2 concentrations, there was some contribution from the RAMP SO_2 sensor. This may be due to cross-

Table 3. Comparison to other published studies.

	Project	Location	Sensor node	Type	N (days)	Time res. (min)	AvgConc (ppb)	Slope	R^2	MAE (ppb)	MBE (ppb)
CO	EuNetAir[1]	Aveiro, PT	AirSensorBox	EC	6	60	330	NR	0.76	90	0
	EuNetAir[1]	Aveiro, PT	NanoEnvi	EC	9	60	330	NR	0.53	100	100
	EuNetAir[1]	Aveiro, PT	Cambridge CAM11	EC	14	60	330	NR	0.87	180	−200
	EuNetAir[1]	Aveiro, PT	AQMesh	EC	15	60	330	NR	0.86	50	0
	CAIRSENSE[2]	Decatur, GA, US	AQMesh	EC	110–111	60	330	NR	0.77–0.87	NR	NR
	CAIRSENSE[2]	Decatur, GA, US	Air Quality Egg	MOS	115–196	60	310	NR	< 0.25	NR	NR
	Castell et al.[3]	Kirkeveien, NO	AQMesh	EC	72	15	NR	0.88*	0.36	150	−150
	Spinelle et al.[4]	Ispra, IT	Figaro, e2V	EC, MOS	85	60	230	1.01–1.38	0.29–0.37	NR	NR
	Cross et al.[5]	Boston, MA, US	ARISense	EC	75	5	–	0.94	0.88	24.8	−10.4
	This study	**Pittsburgh, PA, US**	**RAMP**	**EC**	**41 [10–108]**	**15**	**270 (± 30)**	**0.86 (± 0.09)**	**0.91 (± 0.05)**	**38 (± 6.5)**	**0.1 (± 0.2)**
NO_2	EuNetAir[1]	Aveiro, PT	Cambridge CAM11	EC	14	60	16	NR	0.84	5.61	−2.3
	EuNetAir[1]	Aveiro, PT	AirSensorBox	EC	7	60	16	NR	0.06	20.2	17.7
	EuNetAir[1]	Aveiro, PT	NanoEnvi	EC	7	60	16	NR	0.57	14.9	13.1
	EuNetAir[1]	Aveiro, PT	ECN_Box_10	EC	11	60	16	NR	0.89	4.95	−1
	EuNetAir[1]	Aveiro, PT	AQMesh	EC	6	60	16	NR	0.89	1.46	0
	EuNetAir[1]	Aveiro, PT	ISAG	MOS	13	60	16	NR	0.02	16.2	349.5
	CAIRSENSE[2]	Decatur, GA, US	Cairclip	EC	194–285	60	11	0.96	< 0.25–0.57	NR	NR
	CAIRSENSE[2]	Decatur, GA, US	AQMesh	EC	110–111	60	10	NR	< 0.25	NR	NR
	CAIRSENSE[2]	Decatur, GA, US	Air Quality Egg	MOS	115–196	60	11	NR	< 0.25	NR	NR
	Duvall et al.[6]	Houston, TX, US	Cairclip	EC	24	60	5.5	0.25	0.01	NR	NR
	Duvall et al.[6]	Denver, CO, US	Cairclip	EC	30	60	5.1	0.04	< 0.01	NR	NR
	Castell et al.[3]	Kirkeveien, NO	AQMesh	EC	72	15	NR	0.2–0.38*	0.24	26.2	13.3
	Esposito et al.[7]	Cambridge, UK	SnaQ	EC	28	1	NR	NR	0.83	1.27	NR
	Spinelle et al.[8]	Ispra, IT	αSense, Citytech	EC	86	60	9	0.64–0.79	0.55–0.59	NR	NR
	Cross et al.[5]	Boston, MA, US	ARISense	EC	89	5	NR	0.81	0.69	3.45	1.20
	This study	**Pittsburgh, PA, US**	**RAMP**	**EC**	**24 [2–56]**	**15**	**12 (± 1.4)**	**0.64 (± 0.11)**	**0.67 (± 0.12)**	**3.48 (± 0.36)**	**−0.4 (± 1.13)**
O_3	EuNetAir[1]	Aviero, PT	AirSensorBox	EC	6	60	17	NR	0.13	22.12	19.2
	EuNetAir[1]	Aviero, PT	NanoEnvi	MOS	9	60	17	NR	0.77	7.66	6.5
	EuNetAir[1]	Aviero, PT	Cambridge CAM11	EC	11	60	17	NR	0.14	21.5	15.7
	EuNetAir[1]	Aviero, PT	AQMesh	EC	6	60	17	NR	0.7	2.4	0
	EuNetAir[1]	Aviero, PT	ISAG	MOS	13	60	17	NR	0.12	360.12	356.1
	CAIRSENSE[2]	Decatur, GA, US	Aeroqual SM50	GSS	168–281	60	18	0.81–0.96	0.82–0.94	NR	NR
	CAIRSENSE[2]	Decatur, GA, US	Cairclip	EC	194–285	60	17	0.68–0.85	0.68–0.88	NR	NR
	CAIRSENSE[2]	Decatur, GA, US	AQMesh	EC	110–111	60	15	NR	< 0.25	NR	NR
	Duvall et al.[6]	Houston, TX, US	Cairclip	EC	24	60	32	0.93	0.80	NR	NR
	Duvall et al.[6]	Denver, CO, US	Cairclip	EC	30	60	46	1.19	0.77	NR	NR
	Castell et al.[3]	Kirkevein, NO	AQMesh	EC	72	15	NR	0.11–0.26*	0.29	19.9	6.8
	Esposito et al.[7]	Cambridge, UK	SnaQ	EC	28	1	NR	NR	0.69	7.45	–
	Spinelle et al.[8]	Ispara, IT	αSense, Citytech	EC	82–84	60	30	1.02–1.12	0.86–0.91	NR	NR
	Cross et al.[5]	Boston, MA, US	ARISense	EC	87	5	NR	0.47	0.39	7.34	0.78
	This study	**Pittsburgh, PA, US**	**RAMP**	**EC**	**38 [11–103]**	**15**	**22 (± 1.4)**	**0.82 (± 0.05)**	**0.86 (± 0.02)**	**3.36 (± 0.41)**	**−0.14 (± 0.46)**

[1] Borrego et al. (2016). [2] Jiao et al. (2016). [3] Castell et al. (2017). [4] Spinelle et al. (2017). [5] Cross et al. (2017). [6] Duvall et al. (2016). [7] Esposito et al. (2016). [8] Spinelle et al. (2015).
EC: electrochemical; MOS: metal oxide sensor; GSS: gas sensitive semiconductor. NR means not reported in manuscript. For RAMP data, bracketed data are range (for N days) or standard deviation (all other metrics) across all the RAMP units.
* values for slopes only provided for a subset of 2 of 24 sensors.

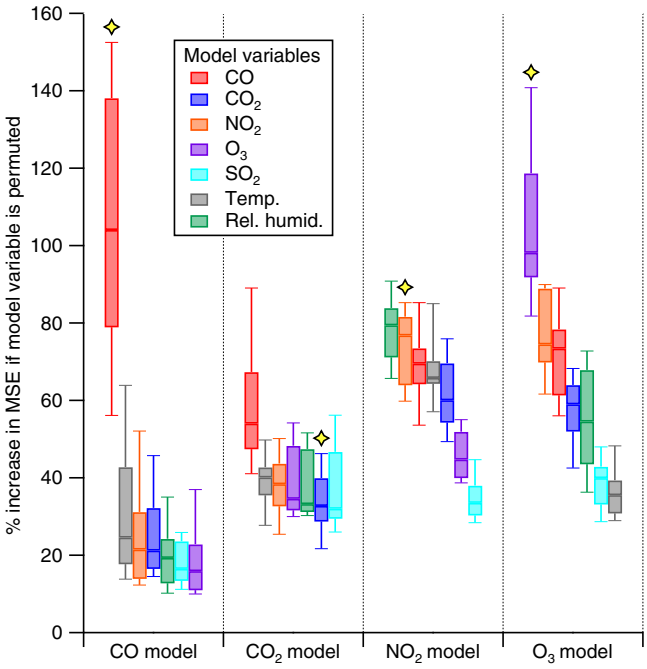

Figure 9. Importance of the explanatory variables to each of the RF models. For each model, the explanatory variables are rank-ordered from most to least important, and the sensor response corresponding to the target analyte is marked with a yellow star. The box plots represent the range of importance across the 10–16 RAMP monitors (whiskers: 10th and 90th percentile; box edges: 25th and 75th percentile). The relative importance is determined by calculating the increase in mean square error if the explanatory variable is permuted (i.e., randomly shuffled).

sensitivities within the SO_2 sensor itself, as the SO_2 sensor may respond to more than ambient SO_2, warranting future investigation. However, in general the SO_2 sensor contributed the least to model performance; thus this sensor could be replaced with a more relevant sensor, such as NO, in future iterations of the RAMP monitor. These findings highlight the value of bundling sensors for measuring a suite of pollutants together, as the different sensors can capture (at least to some extent) cross-sensitivities to other pollutants and improve the model performance for other sensors.

4.3.3 RF model performance as a function of ambient concentration

In Sect. 4.2, predicted concentrations were normalized to average reference monitor concentration to quantitatively compare differences between the calibration models (CvMAE). To evaluate the RF model performance at different reference concentrations, the testing data were divided into deciles for which the median reference monitor concentration, the absolute residual, and the residual normalized to the reference monitor concentration were calculated (Fig. 10). For all species, the RF models tended to overestimate at lower concentrations and underestimate at the highest concentrations. For the CO RF model, the normalized residual is within 10 % of the reference monitor concentration by the 20th percentile of the data (> 100 ppb) and continues to improve until the 50th percentile, when it plateaus at a normalized residual of about 5 %. The US EPA requires a limit of detection of 100 ppb for CO instruments used for regulatory monitoring (United States Environmental Protection Agency, 2014); thus our performance meets that goal. In the top decile, the average absolute CO residual for the RF models approximately doubles, but the relative error is still around 5 %. However, the top decile spans the broadest concentration range due to the lognormal shape of the CO concentration distribution, and these points are difficult to capture in training data sets.

For the CO_2 RF model, agreement with the reference monitor data is within a few percent up to the 90th percentile, when agreement drops to within 5 %. This is possibly due to the RF model actively supressing high CO_2 sensor signals, as the sensor is prone to reading erroneously high concentrations during rain events. Additionally, the top decile of the data spans a wide range of CO_2 concentrations due to the lognormal shape of the CO_2 distribution. As with CO, the NO_2 RF model agreement with the reference monitor plateaus around the 50th percentile mark; however, the NO_2 RF model error exceeds 100 % for the lowest decile (< 5 ppb), suggesting an effective sensitivity of the sensor of 5 ppb. For the O_3 RF model, the effective sensitivity is also around 5 ppb; when the average reference monitor concentration increased from 5 ppb to 10 ppb (from first to second decile), the normalized residual decreased from over 100 % to about 20 %. The US EPA limit of detection for federal regulatory monitors is 10 ppb for both NO_2 and O_3, suggesting that, as with CO, the RF model performance is within 20 % of regulatory standards (United States Environmental Protection Agency, 2014).

Systematic underprediction at the highest concentrations was also observed and is likely a consequence of the training data set used to fit the RF model. Unless the range of concentrations in the training data encompasses the range of concentrations during model testing, there will be underpredictions for concentrations in exceedance of the training range due to the RF model's inability to extrapolate. This is also what causes the horizontal feature for some RAMP monitors at high O_3 concentrations in Fig. 5, as the model will not predict beyond its training range. Additionally, the performance of the RF model is sensitive to the number of data points at a given concentration and the model performance. To build a robust model, many data points are required at a given concentration to probe the extent of the ambient air pollutant matrix. In this study, the training windows were dispersed throughout the collocation period to ensure good agreement of gas species and meteorological conditions during both the training and testing windows (see Supplement). The RF model may not work well in cases where such a diverse collocation window is not possible or where concentra-

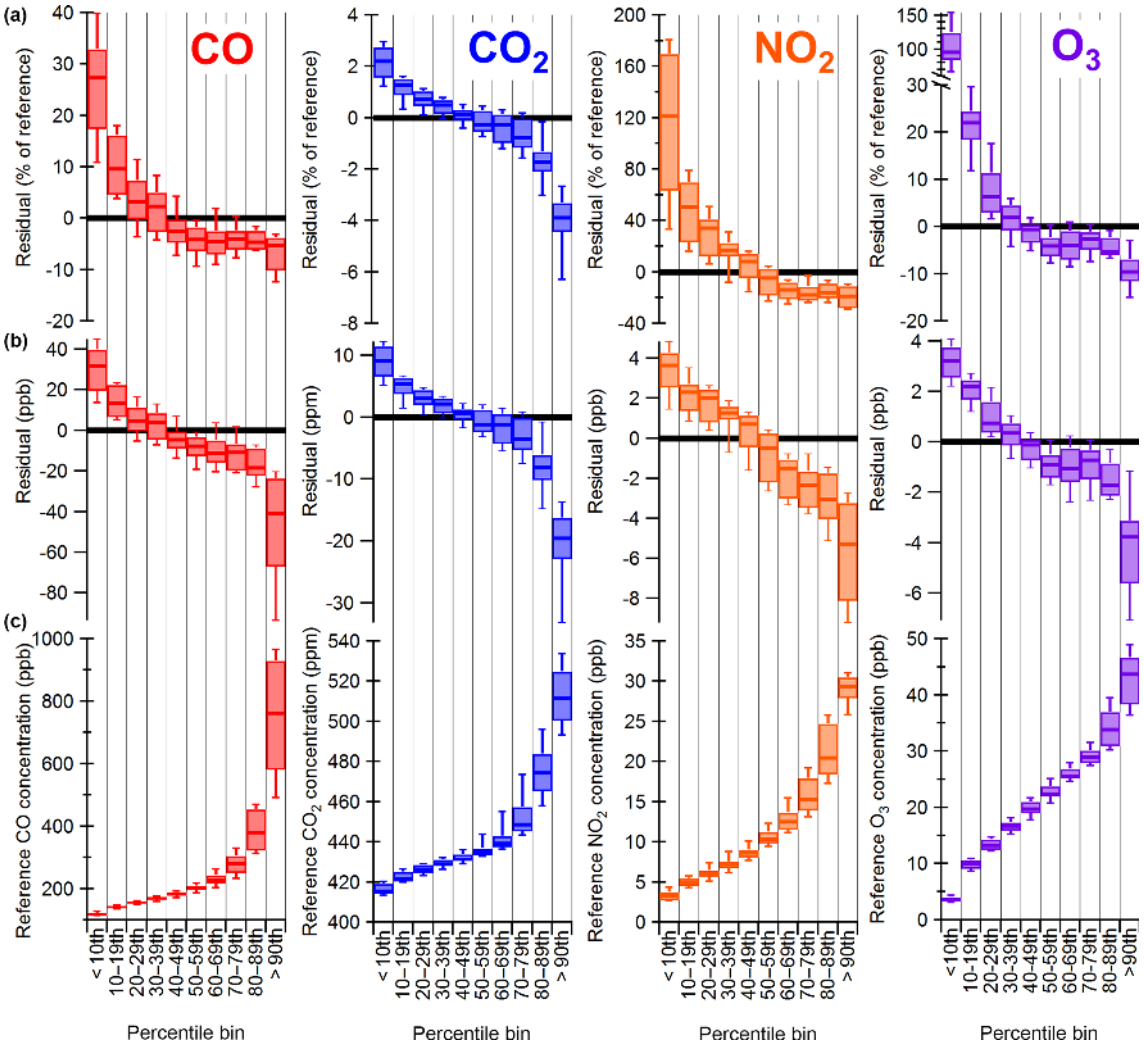

Figure 10. Box plots from the 10–16 RAMP monitors of median concentrations measured by monitors (**c**) and median model residuals (**b**) and model residuals normalized to the reference concentration (**a**) for each pollutant, divided into deciles. The box plots provide the range of medians by the different RAMP monitors.

tions are routinely expected to exceed the training window. In such situations, hybrid calibration models such as combined RF–MLR, where MLR is used for concentrations higher than the RF training window range, may be suitable as MLR tends to perform better when concentrations are higher. An example of this approach is provided by Hagan et al. (2017).

To illustrate the impact of the number of training data points on the RF model, we binned the data for the representative RAMP (RAMP #1) by concentration, and the average concentration measured by the reference monitors was plotted against the average concentration from the calibrated RAMP (Fig. 11). The uncertainty in the RF model was plotted as the standard deviation of the model solutions from the 500 trees, and the bins were color-coded by the number of data points within each bin. Figure 11 illustrates that, for every pollutant, agreement with the reference monitor and uncertainty in the model prediction were larger for concentration bins containing fewer than 10 data points. This disproportionately impacted the upper end of the pollutant distribution where fewer data points were collected due to the intermittent and variable nature of high-pollution episodes. This suggests that a minimum of 10 data points at a given concentration are needed to adequately train the RF model, which may inform future RF model building. At NO_2 concentrations below 5 ppb, deviations from the 1 : 1 line were also observed despite the training data set containing more than 100 data points at these concentrations. As was concluded from Fig. 10, 5 ppbv appears to be the sensitivity limit of these low-cost sensors for NO_2.

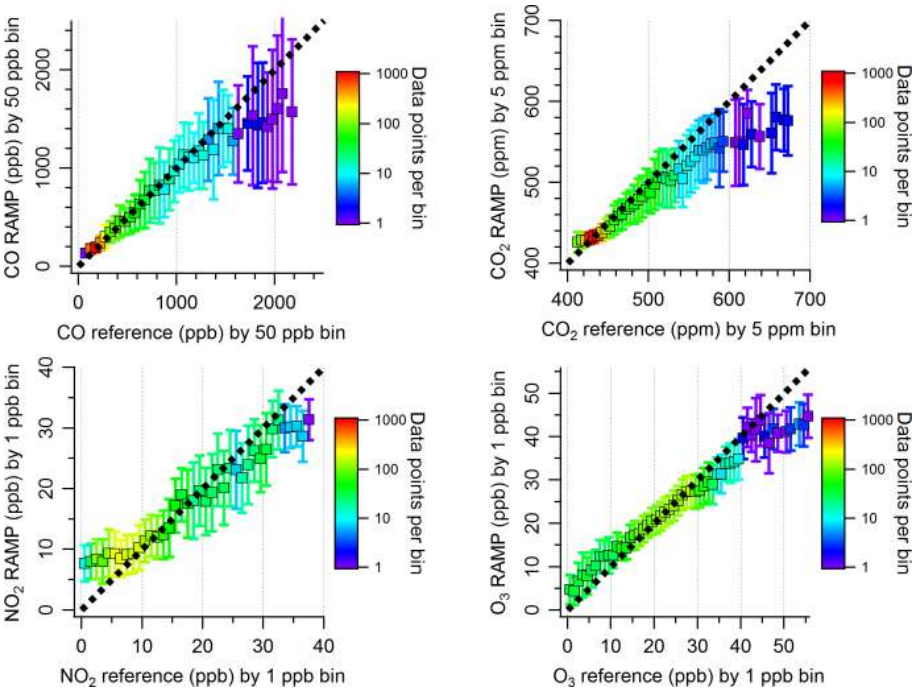

Figure 11. Illustrating the range of predictions from the 500 trees for RAMP #1. The testing data were binned and averaged. The concentration measured by the calibrated RAMP monitors is then plotted against the average concentration from the reference monitor. The error bars represent the standard deviation of the answers from the 500 trees, and the bins are color-coded by the number of data points within each bin. The dashed black line is the 1 : 1 line.

4.4 Comparison of results to other published studies

In this section, we compare the performance of our RF models to results from other recent studies, including the EuNetAir project in Portugal (Borrego et al., 2016) and EPA Community Air Sensor Network (CAIRSENSE) project (Jiao et al., 2016). Additionally, a handful of studies have tested the field performance of low-cost sensors both "out of the box" with factory calibrations (Castell et al., 2017; Duvall et al., 2016) and after a machine-learning-based calibration (Cross et al., 2017; Esposito et al., 2016; Spinelle et al., 2015, 2017). We compare the performance of our RF models to these studies in Table 3. While several low-cost sensor calibration studies have investigated calibration models within laboratory environments (Masson et al., 2015a; Mead et al., 2013; Piedrahita et al., 2014; Williams et al., 2013), we have elected to limit our comparison to field data.

There was not a substantial difference in performance of the RF-model-calibrated vs. LAB-calibrated RAMP for CO, and performance was best for this pollutant on the out-of-the-box factory-calibrated performance assessments in EuNetAir and CAIRSENSE, suggesting that rigorous calibration models may not be critical for CO. However, the RAMP CO RF model did provide improved performance (smallest MAE, 38 ppb) at lower average concentrations compared to the EuNetAir study. Similarly, the out-of-the-box performance of the CO sensors tested as part of CAIRSENSE and by the 24 AQMesh sensors tested in Castell et al. (2017) was poorer than the RF-model-calibrated RAMP. Of those studies that used an advanced algorithm to calibrate the sensors (Cross et al., 2017; Spinelle et al., 2017), the CO RF model resulted in the highest R^2 values and slightly lower slopes; the slope closest to 1 was reported by Cross et al. (2017).

For NO_2, the performance of out-of-the-box low-cost sensors varied widely, and half the sensors in the EuNetAir study (Borrego et al., 2016) reported errors larger than the average ambient concentrations. While the quality of the baseline gas sensing unit remains critical (in which case no calibration should work), we suggest that advanced calibration models, such as those using machine learning, may be critical for accurate measurements of ambient NO_2. Furthermore, sensor performance was correlated with average ambient concentration; studies in areas with higher NO_2 concentrations had the best performance, consistent with our observations (Fig. 10). For studies using advanced NO_2 sensor calibration models (Cross et al., 2017; Esposito et al., 2016; Spinelle et al., 2015), Esposito et al. (2016) had the best performance, with a MAE of < 2 ppb; however, this evaluation was done in a location with high NO_2 concentrations, 45 ppbv (Air Quality England, 2015), more than 3 times higher than the 12 ppbv in Pittsburgh. In addition, they only evaluated one sensor array, so the robustness of the approach is unknown. In our study, the MAEs across the NO_2 RF model RAMP monitors ranged from 2.6 to 3.8 ppb, which is almost as good as Esposito et

al. (2016), but at less than one-third the ambient concentrations. The slope of the HDMR model for NO_2 of Cross et al. (2017) does exceed that of the RAMP RF model, but the R^2 and MAE values are similar between both studies. Similarly, the annual average NO_2 concentrations in 2015 were 15 ppb at the Massachusetts regulatory site used as a reference in Cross et al. (Massachusetts Department of Environmental Protection, 2016), 3 ppb higher than the average concentration observed in our study. As shown in Fig. 10, an increase of a few ppb of NO_2 can result in almost 100 % reductions in relative residuals in our model, potentially explaining discrepancies in the slope between our study and Cross et al. (2017). Furthermore, for identical factory-calibrated sensors out of the box, such as the Cairclip and AQMesh, a 5 ppb increase in average NO_2 concentration results in R^2 values more than doubling. As such, the excellent performance of the RF model for NO_2 at average ambient concentrations of 12 ppbv shows promise.

For O_3, the RF model, the calibrated data from Spinelle et al. (2015), and the measurements from the Aeroqual SM50 (Jiao et al., 2016) performed the best. Good performance from the Aeroqual when measuring NO_2 has also been previously observed (Delgado-Saborit, 2012). However, the results were the most consistent across the RAMP monitors calibrated with RF models, with relative standard deviations of < 20 % across the 16 RAMP monitors for all markers of statistical performance. This performance consistency also holds for the CO and NO_2 RF models. The O_3 RF models were built in Pittsburgh, PA, which has historically had issues with National Ambient Air Quality Standards (NAAQS) ozone compliance; thus while our model was seemingly one of the most accurate and robust, some of this performance may be attributed to the higher ambient O_3 concentrations. From this comparison, we conclude that the RAMP monitor calibrated with a RF model is unique in that it is more accurate when considering the combined suite of pollutants (i.e., all pollutants were accurately measured), it is consistent between many units (< 20 % relative standard deviation in performance metrics across 10–16 monitors), and it is precise even at lower ambient concentrations.

4.5 RF-model-calibrated RAMP performance in a monitoring context

We further assess the RAMP monitor performance against three metrics: (1) comparison of a RAMP monitor calibrated at Carnegie Mellon against an independent set of regulatory reference monitors at the Allegheny County Health Department, (2) NAAQS compliance, and (3) suitability for exposure measurements as per the US EPA Air Sensor Guidebook (Williams et al., 2014). We also demonstrate the benefit of improved performance of the RF models in a real-world deployment at two nearby sites in Pittsburgh, PA.

From February through May 2017, a RAMP monitor calibrated at the Carnegie Mellon campus was deployed at ACHD to test the performance of the RAMP monitor relative to an independent reference monitor (Fig. 12). The ACHD site reports data hourly, so RAMP data were down-sampled to hourly averages, and the CO, NO_2, and O_3 concentrations were compared (no measurement of CO_2 is made at ACHD). For all pollutants, R^2 was ≥ 0.75 (CO: 0.85; NO_2: 0.75; O_3: 0.92) and points were clustered around the 1 : 1 line. NO_2 performed the most poorly, with a large cluster of points in the 5–10 ppb range, where the model is known to underperform. The MAE was 49 ppb (17 % CvMAE) for CO, 4.7 ppb for NO_2 (39 % CvMAE), and 3.2 ppb for O_3 (16 % CvMAE), in line with the performance metrics in Fig. 6. At the time of this submission, RAMP monitors have been collocated with reference monitors at three additional ACHD sites; these comparisons will be the subject of a forthcoming publication.

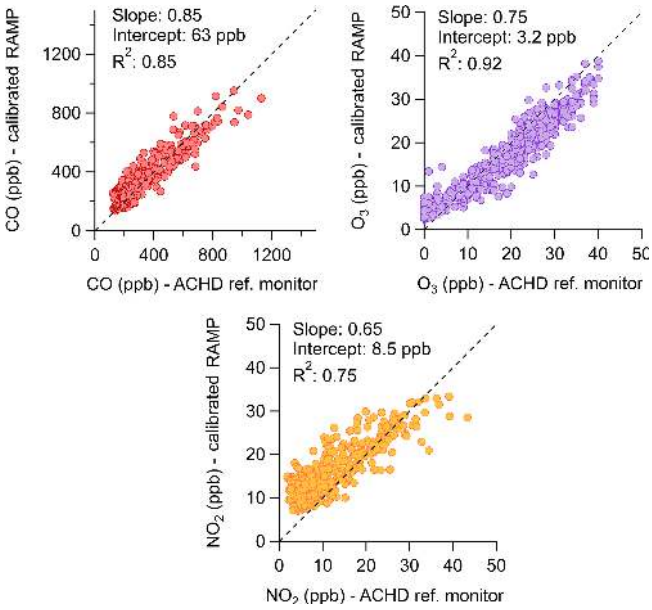

Figure 12. Comparison of CO, NO_2, and O_3 hourly average concentrations measured by a collocated RAMP monitor and the reference monitors at the Allegheny County Health Department (ACHD). The RAMP monitor was first calibrated on the Carnegie Mellon campus prior to deployment.

Regulatory agencies must also report compliance with NAAQS. In this study, the time resolution and methods used to assess the effectiveness of the RF models (15 min) do not match the metrics used for NAAQS. For example, the NAAQS standard for O_3 is based on the maximum daily maximum 8 h average, and compliance for NO_2 is based on the 98th percentile of the daily maximum 1 h averages. While acknowledging that the RAMP monitor collocation period was shorter than typical NAAQS compliance periods (e.g., annually for O_3 and across 3 years for NO_2), it is still worth characterizing the RAMP performance using the LAB, MLR, and RF models (Fig. 13). For the representative RAMP mon-

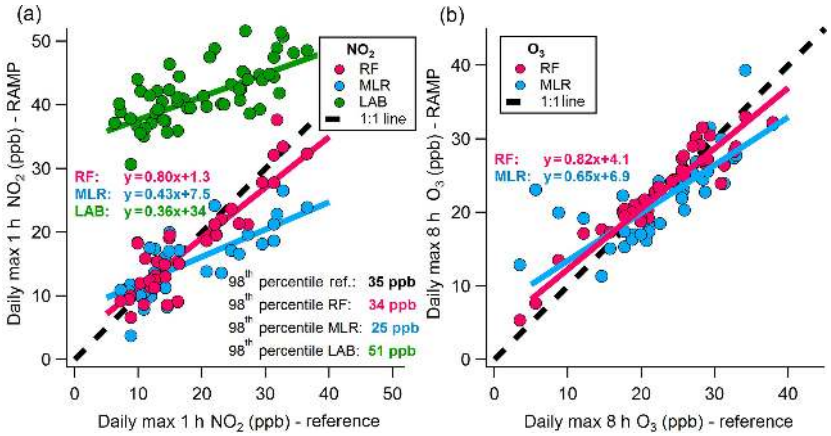

Figure 13. Performance of one representative RAMP monitor (RAMP #1) for NAAQS compliance metrics (O_3: daily max 8 h; NO_2: 98th percentile of daily max 1 h averages). **(b)** Comparison of daily 8 h maximum reference monitor ozone concentrations (x axis) to MLR and RF models. **(a)** Comparison of daily 1 h maximum reference monitor concentrations versus the LAB, MLR, and RF models. The NO_2 standard is the 98th percentile of the daily 1 h maximums.

itor used previously (RAMP #1), daily maximum 8 h O_3 was in good agreement between the RF-calibrated RAMP and the reference monitor, with all data points falling roughly along the 1 : 1 line (slope: 0.82; 95 % CI: 0.81–0.83), while for the MLR model, concentrations were skewed slightly low (slope: 0.65; 95 % CI: 0.63–0.67). For NO_2, the 98th percentile of the daily maximum 1 h averages was 34 ppb for the RF model versus 35 ppb measured using a reference monitor compared to 25 ppb for the MLR model and 51 ppb for the LAB model. The RF model was substantially closer to the reference monitor estimate, and the underestimation was only by 1 ppb. Other RF-model-calibrated RAMP monitors performed similarly, all agreeing within 5 ppb.

Air sensor performance goals by application area are also provided by the US EPA Air Sensor Guidebook (Williams et al., 2014). The performance criteria include maximum precision and bias error rates for applications ranging from education and information (Tier I) to regulatory monitoring (Tier V). The precision estimator is the upper bound of a 90 % confidence interval of the coefficient of variation (CV) and the bias estimator is the upper bound of a 95 % confidence interval of the mean absolute percent difference between the sensors and the reference (full equations in the Supplement). An overarching goal of RAMP monitor deployments is to use low-cost sensor networks to quantify intra-urban exposure gradients; thus our benchmark performance was Tier IV (personal exposure), which recommends that low-cost sensors have precision and bias error rates of less than 30 %. For the testing (withheld) periods, we compared the performance of the RF, MLR and LAB models for all the RAMP monitors used in this study to the precision and bias estimators recommended by the US EPA (Fig. 14). The performance across the RAMP monitors was summarized using box plots, and only the RF-model-calibrated RAMPs are suitably precise and accurate for Tier IV (personal exposure) monitoring across CO, NO_2, and O_3. Furthermore, both RF-model-calibrated CO and O_3 RAMP monitor measurements were below the even more stringent Tier III (supplemental monitoring) standards, which recommends precision and bias error rates of < 20 %. The RF model NO_2 RAMP measurements may reach Tier III in locations with higher NO_2 concentrations.

To demonstrate the improved performance of the RF models in a real-world context, two of the RAMP monitors used in the evaluation study were deployed for a 6-week period at two nearby sites in Pittsburgh, PA. One RAMP monitor was located on the roof of a building at the Pittsburgh Zoo in a residential urban area, and another was placed approximately 1.5 km away at a near-road site located within 15 m of Highway 28 in Pittsburgh (Fig. 15). NO_2 concentrations are known to be elevated up to 200 m away from a major roadway compared to urban backgrounds due to the reaction of fresh NO in vehicle exhaust with ambient O_3 (Zhou and Levy, 2007). Figure 15 shows the diurnal profiles of the RAMP monitors at the two locations evaluated using the RF and MLR models. The RF model indicates an NO_2 enhancement of approximately 6 ppb at the near-road site (Fig. 15, red trace) compared to the nearby urban residential site (Fig. 15, blue trace), and there are notable increases in NO_2 during morning and evening rush hour periods, as expected. However, applying the MLR model to the RAMP data reveals no significant difference between the two sites (Fig. 15, bottom diurnal). In fact, the MLR model predicts negative concentrations during the day. The results of this preliminary deployment suggest that the RF-model-calibrated RAMP monitors could be suitable for quantification of intra-urban pollutant gradients.

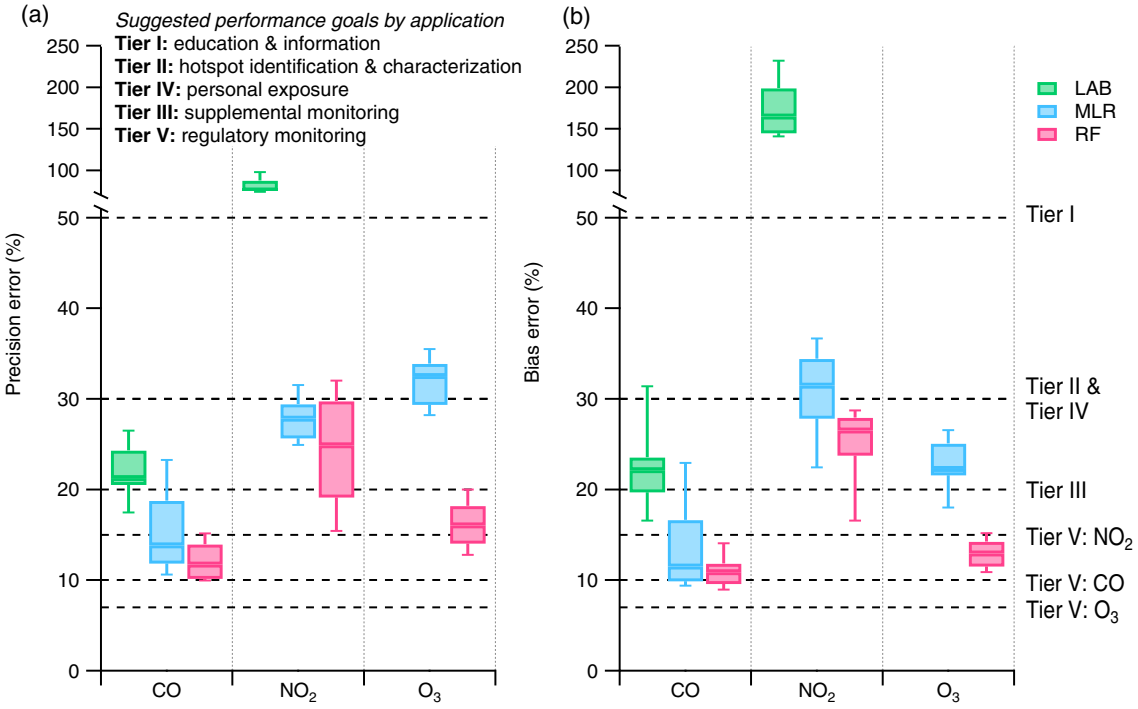

Figure 14. Precision **(a)** and bias **(b)** estimates of RAMP monitors calibrated using LAB, MLR, and RF models compared to the suggested performance goals by application as recommended in the EPA Air Sensor Guidebook. The precision estimator is the upper bound of the coefficient of variation (upper bound of the relative standard deviation, RSD). The box plots are the range of performance across the calibrated RAMP monitors (testing data only). The calibrated RAMP monitors meet the recommended error limits for exposure (Tier IV).

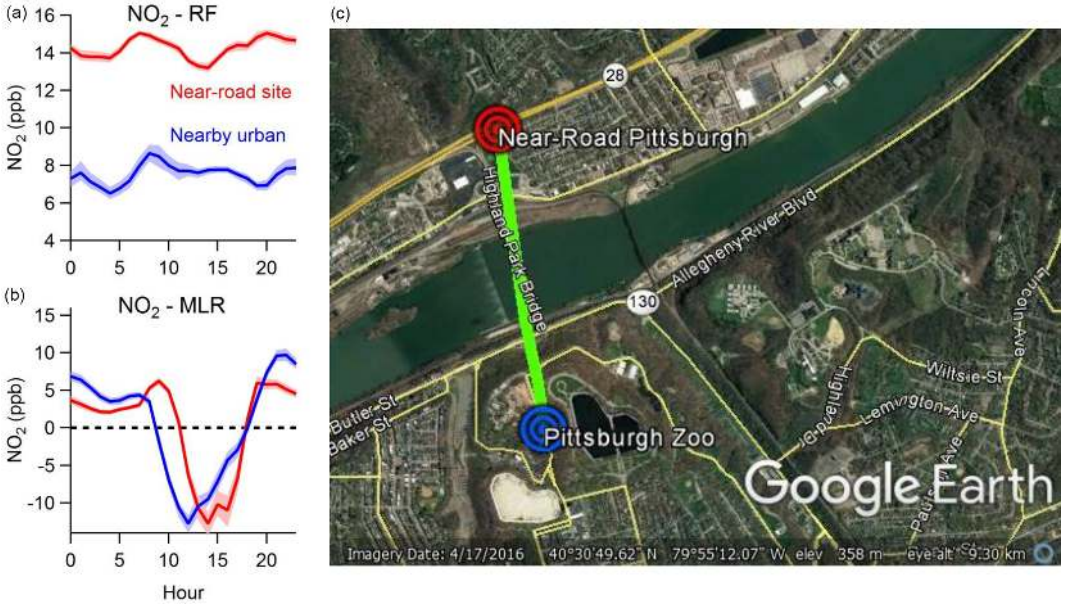

Figure 15. Diurnal NO_2 patterns at two nearby sites (one urban, one near-road) measured by RAMP monitors calibrated using RF models **(a)** or MLR models **(b)**. **(c)** Satellite view of the two sites, which were ∼ 1.5 km apart. The urban site was at the Pittsburgh Zoo, and the near-road site was within 15 m of Highway 28.

5 Conclusions

This study demonstrates that the RF model applied to the RAMP low-cost sensor package can accurately characterize air pollution concentrations at the low levels typical of many urban areas in the United States and Europe. The fractional error of the models at a 15 min time resolution was $< 5\,\%$ for CO_2, approximately 10–15 % for CO and O_3, and approximately 30 % for NO_2, corresponding to mean absolute errors of 10 ppm, 38 ppb, 3.4 ppb, and 3.5 ppb, respectively. This performance meets the recommended precision and accuracy error metrics from the US EPA Air Sensor Guidebook for personal exposure (Tier IV) monitoring. We demonstrate that this degree of sensitivity allows quantification of intra-urban gradients. Furthermore, the calibration models were well constrained across 10–16 RAMP units (all performance metrics $< 20\,\%$ relative standard deviation) and showed minimal degradation over the duration of the collocation study (August 2016 to February 2017),

While the iteration of the RAMP monitor used in this study was equipped with an SO_2 sensor, no calibration model was possible due to SO_2 concentrations at our supersite being below reference instrument detection limits. One feature of the RAMP monitor is that the sensors are modular and can be readily replaced. The assessment of explanatory variable importance combined with the sub-detection-limit levels of SO_2 during the study suggests that the RAMP monitor did not substantially benefit from the presence of the SO_2 sensor in this urban background environment. Future iterations of the RAMP monitor will be equipped with NO sensors, which may be more relevant in an urban context.

The RF models described here were built on 4 weeks of training data equally distributed in 3.5-day periods throughout the entire collocation (examples shown in Fig. S11). This is nominally equivalent to 3–4 days of calibration every 2 months. As previously mentioned, the low-cost sensor modules within the RAMP monitors can be readily replaced, and as such, we recommend for a large urban deployment to prepare a set of sensors at a regulatory monitoring site and to exchange sensors as they malfunction or as calibration models drift. Since the completion of this study, the sensors have been deployed in Pittsburgh for over 4 months, and changes in the calibration models over longer periods of deployment (1 year or more) will be discussed in a future work. Additionally, the sensors were first opened in July 2016 and characterized over the first 7 months of exposure to ambient environments. During this period, no significant temporal drift or sensor degradation was observed, but longer observational studies are likely needed to characterize sensor decay and end of life.

The calibration models were developed in Pittsburgh, which had higher O_3 and lower NO_2 than several published field-based calibrations and measurements with low-cost sensors. Our results and those of other studies demonstrate that low-cost sensor performance generally increases with increasing ambient concentration, but despite this, the RF models for NO_2 had the second-lowest mean absolute error (< 4 ppbv) even at low NO_2 concentrations. The good performance of the RF models across all pollutants can likely be attributed to the ability of the RF models to account for pollutant and meteorological cross-sensitivities, highlighting the importance of building multipollutant sensor packages.

Overall, we conclude that, with careful data management and calibration using advanced machine learning models, low-cost sensing with the RAMP monitors may significantly improve our ability to resolve spatial heterogeneity in air pollutant concentrations. Developing highly resolved air pollutant maps will assist researchers, policymakers, and communities in developing new policies or mitigation strategies to enhance human health. Going forward, a random-forest-calibrated RAMP network of up to 50 nodes will be deployed in Pittsburgh, PA. This robustly calibrated network will help support better epidemiological models, aid in policy planning, and identify areas where more assessment is needed.

Data availability. Reference monitor data, RAMP raw signal data, calibrated RAMP data for both training and testing windows, and data needed to recreate Figs. 4 through 15 are provided online at https://doi.org/10.5281/zenodo.1146109 (Zimmerman et al., 2018). The random forest calibration models and associated R scripts are not available online due to a provisional patent application.

The Supplement related to this article is available online at https://doi.org/10.5194/amt-11-291-2018-supplement.

Competing interests. Author J. Gu is the CEO of SenSevere, the developer and manufacturer of the RAMP hardware. The extent of J. Gu's involvement was solely in development management and improvement of the hardware in the RAMP monitors, not in data analysis. Authors N. Zimmerman and R. Subramanian may in the future act as consultants for SenSevere on low-cost sensor calibration. The data output from the SenSevere hardware in conjunction with the calibration algorithms presented in this paper yields significantly more accurate measurements than previously reported, and the combination is the subject of provisional patent application. The authors declare no other competing interests.

Acknowledgements. Funding for this study was provided by the Environmental Protection Agency (assistance agreement nos. RD83587301 and 83628601) and the Heinz Endowment Fund (grants E2375 and E3145). Naomi Zimmerman's funding was provided by the NSERC Postdoctoral Fellowship (PDF-487660-2016). The authors also wish to thank Aja Ellis and Joshua S. Apte for helpful conversations, and Misha Schurman Boehm for her assistance with the laboratory calibrations.

Edited by: Dominik Brunner
Reviewed by: two anonymous referees

References

Air Quality England: Air Pollution Report, 1st January to 31st December 2016, Cambridge Parker Street (Site ID: CAM 1), 1–4, available at: http://www.airqualityengland.co.uk/site/statistics?site_id=CAM1 (last access: 22 June 2017), 2015.

Bart, M., Williams, D. E., Ainslie, B., McKendry, I., Salmond, J., Grange, S. K., Alavi-Shoshtari, M., Steyn, D., and Henshaw, G. S.: High density ozone monitoring using gas sensitive semi-conductor sensors in the lower Fraser valley, British Columbia, Environ. Sci. Technol., 48, 3970–3977, https://doi.org/10.1021/es404610t, 2014.

Borrego, C., Costa, A. M., Ginja, J., Amorim, M., Coutinho, M., Karatzas, K., Sioumis, T., Katsifarakis, N., Konstantinidis, K., De Vito, S., Esposito, E., Smith, P., Andre, N., Gerard, P., Francis, L. A., Castell, N., Schneider, P., Viana, M., Minguillon, M. C., Reimringer, W., Otjes, R. P., von Sicard, O., Pohle, R., Elen, B., Suriano, D., Pfister, V., Prato, M., Dipinto, S., and Penza, M.: Assessment of air quality microsensors versus reference methods: The EuNetAir joint exercise, Atmos. Environ., 147, 246–263, https://doi.org/10.1016/j.atmosenv.2016.09.050, 2016.

Breiman, L.: Random Forests, Mach. Learn., 45, 5–32, 2001.

Castell, N., Dauge, F. R., Schneider, P., Vogt, M., Lerner, U., Fishbain, B., Broday, D., and Bartonova, A.: Can commercial low-cost sensor platforms contribute to air quality monitoring and exposure estimates?, Environ. Int., 99, 293–302, https://doi.org/10.1016/j.envint.2016.12.007, 2017.

Cross, E. S., Williams, L. R., Lewis, D. K., Magoon, G. R., Onasch, T. B., Kaminsky, M. L., Worsnop, D. R., and Jayne, J. T.: Use of electrochemical sensors for measurement of air pollution: correcting interference response and validating measurements, Atmos. Meas. Tech., 10, 3575–3588, https://doi.org/10.5194/amt-10-3575-2017, 2017.

Delgado-Saborit, J. M.: Use of real-time sensors to characterise human exposures to combustion related pollutants, J. Environ. Monit., 14, 1824–1837, https://doi.org/10.1039/C2EM10996D, 2012.

De Vito, S., Massera, E., Piga, M., Martinotto, L., and Di Francia, G.: On field calibration of an electronic nose for benzene estimation in an urban pollution monitoring scenario, Sensor. Actuat. B-Chem., 129, 750–757, https://doi.org/10.1016/j.snb.2007.09.060, 2008.

De Vito, S., Piga, M., Martinotto, L., and Di Francia, G.: CO, NO_2 and NO_x urban pollution monitoring with on-field calibrated electronic nose by automatic bayesian regularization, Sensor. Actuat. B-Chem., 143, 182–191, https://doi.org/10.1016/j.snb.2009.08.041, 2009.

Duvall, R. M., Long, R. W., Beaver, M. R., Kronmiller, K. G., Wheeler, M. L., and Szykman, J. J.: Performance evaluation and community application of low-cost sensors for ozone and nitrogen dioxide, Sensors (Switzerland), 16, 1698, https://doi.org/10.3390/s16101698, 2016.

Esposito, E., De Vito, S., Salvato, M., Bright, V., Jones, R. L., and Popoola, O.: Dynamic neural network architectures for on field stochastic calibration of indicative low cost air quality sensing systems, Sensor. Actuat. B-Chem., 231, 701–713, https://doi.org/10.1016/j.snb.2016.03.038, 2016.

Hagan, D. H., Issacman-Vanwertz, G., Franklin, J. P., Wallace, L. M. M., Kocar, B. D., Heald, C. L., and Kroll, J. H.: Calibration and assessment of electrochemical air quality sensors by co-location with reference-grade instruments, Atmos. Meas. Tech. Discuss., https://doi.org/10.5194/amt-2017-296, in review, 2017.

Hitchman, M. L., Cade, N. J., Kim Gibbs, T., and Hedley, N. J. M.: Study of the Factors Affecting Mass Transport in Electrochemical Gas Sensors, Analyst, 122, 1411–1417, https://doi.org/10.1039/a703644b, 1997.

Jiao, W., Hagler, G., Williams, R., Sharpe, R., Brown, R., Garver, D., Judge, R., Caudill, M., Rickard, J., Davis, M., Weinstock, L., Zimmer-Dauphinee, S., and Buckley, K.: Community Air Sensor Network (CAIRSENSE) project: evaluation of low-cost sensor performance in a suburban environment in the southeastern United States, Atmos. Meas. Tech., 9, 5281–5292, https://doi.org/10.5194/amt-9-5281-2016, 2016.

Jolliff, J. K., Kindle, J. C., Shulman, I., Penta, B., Friedrichs, M. A. M., Helber, R., and Arnone, R. A.: Summary diagrams for coupled hydrodynamic-ecosystem model skill assessment, J. Marine Syst., 76, 64–82, https://doi.org/10.1016/j.jmarsys.2008.05.014, 2009.

Kuhn, M., Wing, J., Weston, S., Williams, A., Keefer, C., Engelhardt, A., Cooper, T., Mayer, Z., Kenkel, B., The R Core Team, Benesty, M., Lescarbeau, R., Ziem, A., Scrucca, L., Tang, Y., Candan, C., and Hunt., T.: caret: Classification and Regression Training, available at: https://cran.r-project.org/package=caret, last access: 23 October 2017.

Lewis, A. and Edwards, P.: Validate personal air-pollution sensors, Nature, 535, 29–31, 2016.

Marshall, J. D., Nethery, E., and Brauer, M.: Within-urban variability in ambient air pollution?: Comparison of estimation methods, Atmos. Environ., 42, 1359–1369, https://doi.org/10.1016/j.atmosenv.2007.08.012, 2008.

Massachusetts Department of Environmental Protection: Massachusetts 2015 Air Quality Report, available at: http://www.mass.gov/eea/docs/dep/air/priorities/15aqrpt.pdf (last access: 23 June 2017), 2016.

Masson, N., Piedrahita, R., and Hannigan, M.: Approach for quantification of metal oxide type semiconductor gas sensors used for ambient air quality monitoring, Sensor. Actuat. B-Chem., 208, 339–345, https://doi.org/10.1016/j.snb.2014.11.032, 2015a.

Masson, N., Piedrahita, R., and Hannigan, M.: Quantification method for electrolytic sensors in long-term monitoring of ambient air quality, Sensors (Switzerland), 15, 27283–27302, https://doi.org/10.3390/s151027283, 2015b.

McKercher, G. R., Salmond, J. A., and Vanos, J. K.: Characteristics and applications of small, portable gaseous air pollution monitors, Environ. Pollut., 223, 102–110, https://doi.org/10.1016/j.envpol.2016.12.045, 2017.

Mead, M. I., Popoola, O. A. M., Stewart, G. B., Landshoff, P., Calleja, M., Hayes, M., Baldovi, J. J., McLeod, M. W., Hodgson, T. F., Dicks, J., Lewis, A., Cohen, J., Baron, R., Saffell, J. R., and Jones, R. L.: The use of electrochemical sensors for monitoring urban air quality in low-cost, high-density networks, Atmos. Environ., 70, 186–203, https://doi.org/10.1016/j.atmosenv.2012.11.060, 2013.

Moltchanov, S., Levy, I., Etzion, Y., Lerner, U., Broday, D. M., and Fishbain, B.: On the feasibility of measuring urban air pollution by wireless distributed sensor networks, Sci. Total Environ., 502, 537–547, https://doi.org/10.1016/j.scitotenv.2014.09.059, 2015.

Nazelle, A. De, Rodríguez, D. A., and Crawford-Brown, D.: Science of the Total Environment The built environment and health?: Impacts of pedestrian-friendly designs on air pollution exposure, Sci. Total Environ., 407, 2525–2535, https://doi.org/10.1016/j.scitotenv.2009.01.006, 2009.

Oshiro, T. M., Perez, P. S., and Baranauskas, J. A.: How Many Trees in a Random Forest?, in: Machine Learning and Data Mining in Pattern Recognition: 8th International Conference, MLDM 2012, Berlin, Germany, July 13–20, 2012. Proceedings, edited by: Perner, P., Springer Berlin Heidelberg, 154–168, 2012.

Pang, X., Shaw, M. D., Lewis, A. C., Carpenter, L. J., and Batchellier, T.: Electrochemical ozone sensors: A miniaturised alternative for ozone measurements in laboratory experiments and air-quality monitoring, Sensor. Actuat. B-Chem., 240, 829–837, https://doi.org/10.1016/j.snb.2016.09.020, 2017.

Pearson, R.: Assessing Variable Importance for Predictive Models of Arbitrary Type, available at: https://cran.r-project.org/web/packages/datarobot/vignettes/VariableImportance.html, last access: 23 October 2017.

Perpinan Lamigueiro, O.: tdr: Target Diagram, available at: https://cran.r-project.org/package=tdr (last access: 25 June 2017), 2015.

Piedrahita, R., Xiang, Y., Masson, N., Ortega, J., Collier, A., Jiang, Y., Li, K., Dick, R. P., Lv, Q., Hannigan, M., and Shang, L.: The next generation of low-cost personal air quality sensors for quantitative exposure monitoring, Atmos. Meas. Tech., 7, 3325–3336, https://doi.org/10.5194/amt-7-3325-2014, 2014.

Pugh, T. A. M., Mackenzie, A. R., Whyatt, J. D., and Hewitt, C. N.: Effectiveness of Green Infrastructure for Improvement of Air Quality in Urban Street Canyons, Environ. Sci. Technol., 46, 7692–7699, 2012.

Strobl, C., Boulesteix, A.-L., Kneib, T., Augustin, T., and Zeileis, A.: Conditional variable importance for random forests, BMC Bioinformatics, 9, 307, doi:10.1186/1471-2105-9-307, 2008.

Snyder, E. G., Watkins, T. H., Solomon, P. A., Thoma, E. D., Williams, R. W., Hagler, G. S. W., Shelow, D., Hindin, D. A., Kilaru, V. J., and Preuss, P. W.: The changing paradigm of air pollution monitoring, Environ. Sci. Technol., 47, 11369–77, https://doi.org/10.1021/es4022602, 2013.

Spinelle, L., Aleixandre, M., and Gerboles, M.: Protocol of evaluation and calibration of low-cost gas sensors for the monitoring of air pollution, Eur. Comm. JRC Techical Reports, EUR 26112, https://doi.org/10.2788/9916, 2013.

Spinelle, L., Gerboles, M., Villani, M. G., Aleixandre, M., and Bonavitacola, F.: Field calibration of a cluster of low-cost available sensors for air quality monitoring. Part A: Ozone and nitrogen dioxide, Sensor. Actuat. B-Chem., 215, 249–257, https://doi.org/10.1016/j.snb.2015.03.031, 2015.

Spinelle, L., Gerboles, M., Villani, M. G., Aleixandre, M., and Bonavitacola, F.: Field calibration of a cluster of low-cost commercially available sensors for air quality monitoring. Part B: NO, CO and CO_2, Sensor. Actuat. B-Chem., 238, 706–715, https://doi.org/10.1016/j.snb.2016.07.036, 2017.

Tan, Y., Lipsky, E. M., Saleh, R., Robinson, A. L., and Presto, A. A.: Characterizing the Spatial Variation of Air Pollutants and the Contributions of High Emitting Vehicles in Pittsburgh, PA, Environ. Sci. Technol., 48, 14186–14194, https://doi.org/10.1021/es5034074, 2014.

United States Environmental Protection Agency: Appendix D, Measurement Quality Objectives and Validation Templates, in: QA Handbook Volume II, 5–12, 2014.

Williams, D. E., Henshaw, G. S., Bart, M., Laing, G., Wagner, J., Naisbitt, S., and Salmond, J. A.: Validation of low-cost ozone measurement instruments suitable for use in an air-quality monitoring network, Meas. Sci. Technol., 24, 065803, https://doi.org/10.1088/0957-0233/24/6/065803, 2013.

Williams, R., Kilaru, V. J., Snyder, E. G., Kaufman, A., Dye, T., Ruttler, A., Russell, A., and Hafner, H.: Air Sensor Guidebook, EPA/600/R-14/159, United States Environmental Protection Agency, 2014.

Zhou, Y. and Levy, J. I.: Factors influencing the spatial extent of mobile source air pollution impacts: a meta-analysis, BMC Public Health, 7, 89, https://doi.org/10.1186/1471-2458-7-89, 2007.

Zimmerman, N., Presto, A., Kumar, S., Gu, J., Hauryliuk, A., Robinson, E., Robinson, A., and Subramanian, R.: A machine learning calibration model using random forests to improve sensor performance for lower-cost air quality monitoring (Version v1), https://doi.org/10.5281/zenodo.1146109, 2018.